Soft Matter

PAPER

View Article Online
View Journal | View Issue

Cite this: *Soft Matter*, 2025, 21, 866

Controlled synthesis of ternary acrylamide/sodium acrylate/polyethyleneglycol hybrids by integrating different clays and fillers: a comprehensive evaluation of structural features†

Rabia Bozbay,[ab] Mertcan Er,[ab] Kübra Kara Ersoy[b] and Nermin Orakdogen*[a]

A series of anionic poly(acrylamide-*co*-sodium acrylate)/poly(ethylene glycol), PAN/PEG, hybrids were conveniently synthesized *via* free radical aqueous polymerization by integrating bentonite, kaolin, mica, graphene and silica, following a simple and eco-friendly crosslinking methodology. A comparative perspective was presented on how integrated nanofillers affect the physicochemical properties of hybrid gels depending on the differences in their structures. Among the five types of nanofillers, bentonite-integrated hybrid gel had the highest water absorbency, while graphene-integrated gel had the lowest. The elastic moduli of hybrid gels with the same content of inorganic component followed the order graphene > silica > mica > kaolin > bentonite. Adding 1.50% (w/v) bentonite to the PAN/PEG matrix increased the elastic modulus by 1.4 times compared to the as-prepared state, while adding the same amount of graphene created a 4.1-fold increase. By decreasing the synthesis temperature of hybrids to cryoconditions, −18 °C, an increase in the modulus of all gels was observed, while the modulus of graphene-doped gels increased from 25.9 kPa to 39.1 kPa. pH-dependent swelling demonstrated that hybrid gels can dynamically bind or release protons in response to changes in surrounding pH and thus abruptly change their overall dimensions. On–off switching behavior as reversible pulsatile swelling in pH 11.2 and deswelling in pH 2.1 showed that hybrid gels exhibit reversible pH-responsiveness following Fickian diffusion of water into the hybrid matrix. The change in pH of the swelling medium caused a 4.5-fold increase in swelling ratio for the silica-doped hybrid gels. The studies in which anionic hybrids were tested to explore adsorption potential for cationic dye methylene blue (MB) showed that adsorbent properties could be tuned to the desired extent by incorporating different fillers. In terms of efficiency among the selected fillers, the maximum efficiency for MB was obtained as 99.2% and 88.60% for hybrids containing graphene and silica, respectively. The adsorption of MB on hybrids was fit to the three-parameter Sips model rather than the two-parameter models. The results introduced a new perspective on the design of ternary hybrid gels that could effectively address both the mechanical and responsive properties of soft materials, providing a platform for subsequent cationic dye adsorption.

Received 13th September 2024,
Accepted 2nd January 2025

DOI: 10.1039/d4sm01090f

rsc.li/soft-matter-journal

Introduction

Recent advances in polymer design and progress in the development of multicomponent gels have opened new possibilities for the development of hybrid-structured materials with enhanced properties. Hybrid nanocomposites differ from other multicomponent systems in that their extraordinary properties are achieved through the entanglements between the polymer chains and the extremely close contact between these chains and integrated nanofillers.[1,2] These structures have been developed in which the properties of clay minerals such as cheapness, availability, environmental friendliness, large surface area and stability are combined with the advantageous properties of polymers such as high adsorption efficiency and better regeneration at nanoscale depending on the modification process. For more specific material synthesis, different nanofillers are incorporated to achieve versatile and outstanding gel properties and reactivity. These nanofillers vary in shape and size from micrometers to nanometers, such as polymeric-components, inorganic/ceramic and carbon-based nanoparticles.[3,4]

[a] *Faculty of Science and Letters, Department of Chemistry, Soft Materials Research Laboratory, Istanbul Technical University, Istanbul, Maslak, 34469, Turkey. E-mail: orakdogen@itu.edu.tr; Tel: +90-212-285-3305*
[b] *Graduate School of Science Engineering and Technology, Department of Chemistry, Istanbul Technical University, Istanbul, 34469, Turkey*

† Electronic supplementary information (ESI) available. See DOI: https://doi.org/10.1039/d4sm01090f

Hybrid design provides a powerful strategy for incorporating nanostructures that provide versatile and customized functionality for nanometer-scale control. To develop safe and environmentally friendly materials, the synthesis of hybrid gels from sustainable green materials has shown improved properties such as mechanical strength, low gas permeability and heat resistance, reduced costs and increased effectiveness in removing various pollutants from wastewater.[5] The chemical compatibility between the functional network and the nanofiller is decisive in developing the multifunctional nanocomposites. The extent of interactions between the nanofiller and polymer network, including hydrogen bonding, van der Waals and electrostatic interactions, is effective in designing optimized materials with synergistic properties. To continuously reinforce the network structure after polymerization and match its properties to the nanoparticles, one or more components with specific functionality can be integrated into the network. The incorporation of inorganic components such as layered silicates; bentonite, mica, kaolin, carbon-based materials graphene and graphene oxide, metal oxide nanoparticles; silica, titanium and aluminum oxides into the polymer matrix is intended to change the physicochemical properties to the desired extent, including swelling and modulation of elasticity with advanced properties useful for micropollutants removal.[6] Since clay polymer hybrids offer easy synthesis in large quantities with improved performances, it is necessary to evaluate the process efficiency on a large scale in the removal of biological, organic and inorganic micropollutants from water/wastewater. The blending of modified polymeric structure and inorganic clays or fillers has led to the emergence of a new class of hybrid materials with microcomposite and nanocomposite structures, depending on the procedure followed.

The properties of hybrid structures differ significantly from the properties of the individual components, which makes them interesting in some cases with dramatic synergistic properties. As reported by Bergaya and coworkers, small amounts of inorganic nanoparticles dispersed in a polymer, typically less than 5%, can significantly improve the polymer properties.[7] Tang and co-workers proposed to prepare kaolin-integrated sodium alginate graft poly(acrylic acid-*co*-acrylamide) SA-*g*-P(AAc-*co*-AAm)/Kln composite hydrogel by adjusting the ratio of AAc : AAm : Kln to 6 : 9 : 1.57 (in g) and showed that the composites were effective in removing Rhodamine B from aqueous solution.[8] Hosseini and coworkers prepared ternary nanocomposite aerogel systems containing carboxymethyl cellulose grafted by polyacrylic acid reinforced with different levels of graphene oxide particles.[9] A significant increase in the storage modulus and thermal stability of nanocomposites was attributed to the presence of graphene oxide. While the average size of pores decreases, the porosity of the nanocomposites is reported to increase with graphene oxide concentration, which is effective in increasing their ability to remove pollutants from water. Dai and coworkers combined 50 mg graphene oxide and 1.0 g bentonite to reinforce polyvinyl alcohol/carboxymethyl cellulose hydrogels.[10] The addition of graphene oxide and/or bentonite increased the thermal stability which was attributed to the improved cross-linked structure and hydrogen bond interactions, while the barrier effect of bentonite contributed to the increase in the thermal stability. Limparyoon and coworkers prepared acrylamide/2-acrylamido-2-methylpropane sulfonic acid copolymer nanocomposites using phyllosilicate mineral mica.[11] The addition of 5–30% (w/w) mica to the copolymer resulted in an interlayer structure and the nanocomposites showed better thermal stability and higher water absorbency compared to the blank copolymer. In another work, Zhang and Wang studied the influences of clay-type on the comprehensive swelling of polyacrylamide/clay composites based on various clays, such as attapulgite, kaolinite, mica, vermiculate and Na-montmorillonite prepared by free-radical aqueous polymerization.[12] The composites incorporated with Na-montmorillonite exhibited higher swelling rate, while those doped with mica showed higher reswelling ability. Jiang and coworkers reported the rheological behavior and secondary networks of polyacrylamide hydrogels filled with different types and contents of hydrophilic silica by *in situ* polymerization.[13] Their results suggested the existence of a non-bonded complexation between the molecular chains and silica, which imparts specific properties to the hydrogel network.

Comparative syntheses using different clays, carbon-based materials, metal oxides or their mixtures have rarely been performed on the same template polymeric structure.[14,15] Recognizing the need to enhance the mechanical resilience of polyacrylamide-based hybrids after polymerization, the study attempted to apply an innovative approach by incorporating nanoparticles into the anionic poly(acrylamide-*co*-sodium acrylate) matrix in the presence of linear poly(ethylene glycol) (PEG) chains *via in situ* polymerization. Hybrid material design has generally focused on the effects of a particular clay type on the swelling and elastic properties of nanocomposites, and these studies have provided perspective on changes in low and high clay content by varying the amount of clay. However, it is unclear how the performance of a hybrid material changes when different clay types are added to the same gel system under the same experimental conditions and whether different inorganic clay types can be applied synergistically to good effect. Nowadays, limited literatures have been reported on the addition of different types of nanoparticles to anionic copolymerized gel systems with semi-interpenetrated structure. Inspired by this idea, anionic sodium acrylate-functionalized gel system containing poly(ethylene glycol) chains was successfully prepared in the presence of different nanoparticles in this study. A concept was established for the synthesis of ternary hybrid gels consisting of different fillers as the inorganic component and site-specific (alkyl)amide and carboxyl groups containing polymeric backbone as the organic counterpart pursuing a simple, green and economic methodology. Based on the literature review, graphene, bentonite kaolin, mica, and silica are selected as five different inorganic components for the development of useful, applicable and environmentally friendly materials in the water treatment process. By varying the polymerization conditions (the type of the nanofiller and

the polymerization temperature), five hybrid samples with different nanofiller loadings were produced. A strategy for ternary hybrid gel design has been promoted to investigate the effect of various inorganic components on the elasticity, swelling and thermal stability of ionically modified polyacrylamide-based nanocomposites. The competitive applicability, swelling, elasticity and structural features of the prepared hybrid gels and the removal of cationically charged pollutants were evaluated by considering various parameters. The main objective is to find the relationship between the composition/structure of ternary hybrid gels and their physicochemical capacities. Here, the hybrid composition is controlled by the polymerization temperature, the change in the microstructure, the type and content of nanoparticles and clays with different plate-like structures are considered as factors affecting the properties of hybrids. Since it contains a ternary polymeric structure and different fillers, the novelty of this work is mainly to provide a perspective on a new approach to compare the hybrid structure in terms of the swelling, elasticity, and adsorption results, while keeping all the experimental parameters constant. The possible adsorption mechanisms for cationic methylene blue dye were evaluated and the equilibrium isotherms and dynamics were discussed depending on the type of nanoparticles added to the structure.

Experimental section

Materials

The main monomer acrylamide (AAm, ≥99%, Merck, Darmstadt, Germany), the anionic comonomer sodium acrylate (NaA, ≥97%, Sigma Aldrich, Darmstadt, Germany), and poly(ethylene glycol) (M_w 2000) (PEG) were purchased from Sigma Aldrich. The tetrafunctional cross-linking agent *N*,*N*-methylenebisacrylamide (BAAm, ≥99%), the redox-initiator system ammonium persulfate (APS, ≥98.0%), and *N*,*N*,*N*′,*N*′-tetramethylethylenediamine (TEMED, ∼99%) were supplied from Merck (Darmstadt, Germany) and used as received. Bentonite nanoclay was supplied from Aldrich, and according to the provider, consists of more than 98% Na-montmorillonite. Mica was purchased from U.S. Geological Survey, Denver, Colorado. The main chemical composition is SiO_2 65.8%, Al_2O_3 15.8%, Fe_2O_3 2.62%, FeO 3.93%, Na_2O 2.05%, K_2O 3.28%, TiO_2 1.01%, CaO 1.40%, and MgO 1.69%. Kaolin (>90%) was provided by Kaolin EAD Company, Turkey. Graphene nanoplatelet, a purity of 99.9%, with the average thickness of 3 nm, diameter of 1.5 μm has a particular 800 $m^2\ g^{-1}$ surface area was purchased from Nanografi Nano Technology Company, Germany. Hydrophilic nano-silica particles of 9–15 nm in size was supplied from Zhejiang Yuda Chemical P.R. China in the form of powder. Sodium phosphate tribasic dodecahydrate ($Na_3PO_4{\cdot}12H_2O$, ≥ 98.0%, Merck, Darmstadt, Germany), hydrochloric acid (HCl, Merck, 37%, Darmstadt, Germany), potassium dihydrogen phosphate (KH_2PO_4, ≥99.0%, Riedel-de Haen, Germany), disodium hydrogen phosphate (Na_2HPO_4, ≥99.0%, Merck, Darmstadt, Germany), sodium chloride (NaCl, ≥99.0%, Merck, Darmstadt, Germany), and calcium chloride ($CaCl_2$, J. T. Baker, Phillipsburg, NJ, USA) were used for pH- and salt-responsive swelling experiments. Ultrapure water obtained from the MILLI-Q Laboratory system was used in hybrid gel syntheses, while distilled and deionized water was used in all swelling experiments.

Synthesis of hybrid PAN/PEG-NC gels by *in situ* filler incorporation

For synthesizing the blank gels, named P(AAm-*co*-NaA)/PEG, 514.5 mg of PEG-2000 was dissolved in 6.0 mL of water by stirring at room temperature (23.7 °C). To maintain AAm/NaA mol ratio fixed at 94/6 (mol%/mol%), 514.5 mg of AAm, and 450 μL of NaA were included and stirred for additional 1 h for homogeneous mixture. Then, 1.0 mL of BAAm stock solution (0.2906 g/20 mL), and 1.0 mL of TEMED stock solution (0.750 mL/20 mL) were included, and the mixture was mixed again for additional 1 h. As the last component, 1.0 mL stock solution of the radical initiator APS (0.16 g/20 mL), was added by setting [APS]/[TEMED] = 1/7 and finally, the reaction mixture was transferred into polypropylene syringes with an inner diameter of 4 mm to obtain cylindrical gel specimens for moduli determination in compression as well as for swelling testing. The concentration of AAm in the reaction mixture was 7.235 mM, and that of NaA was 0.476 mM. The amount of BAAm in the synthesis was chosen as 14.5 mg in order to keep the crosslinker ratio *X*, which is defined as the molar ratio of the crosslinker agent BAAm to the total monomers (AAm + NaA), constant at 1/82. In this way, the total monomer concentration was adjusted to be 5.73%. The concentrations of initiator APS and the activator TEMED were characterized as molar ratio [APS]/[AAm] = 0.5 and [TEMED]/[AAm] = 3.5, respectively, according to the neutral monomer content. For the preparation of ternary hybrid gels, the filler, 1.50% (w/v), was first dispersed in 6.0 mL of water well for 4 h followed by addition of linear PEG-2000 chains, monomers; AAm, NaA and BAAm with stirring for another half hour.

Table S1 (ESI†) presents the chemical composition and basic properties of clay minerals used in nanocomposite synthesis in a comparative manner, while Scheme 1 shows the optical views of the aqueous dispersion of bentonite (Bnt), kaolin (Kln), mica, silica (Slc), and graphene (Grn) prepared for the synthesis. After addition of TEMED and APS stock solutions, the polymerization with *in situ* mixing of filler with these monomers was performed in a similar way as in the case of polymerization for the unfilled blank gel. In both cases, the polymerization reaction was conducted at 24 °C for 48 h for the preparation of hydrogels (named Hgs) *via* free-radical crosslinking copolymerization and at −18 °C for the cryogels (named Cgs) *via* freezing-induced cryogelation. The compositions of the ternary hybrids including content of fillers, concentration of monomers AAm, NaA, and BAAm in the reaction mixture were given in Table S2 (ESI†). For the present system, filler-free blank P(AAm-*co*-NaA)/PEG gels were named as PAN/PEG, while the filler-integrated hybrid gels were named as PAN/PEG-NC, in which A is used for AAm, N for anionic monomer

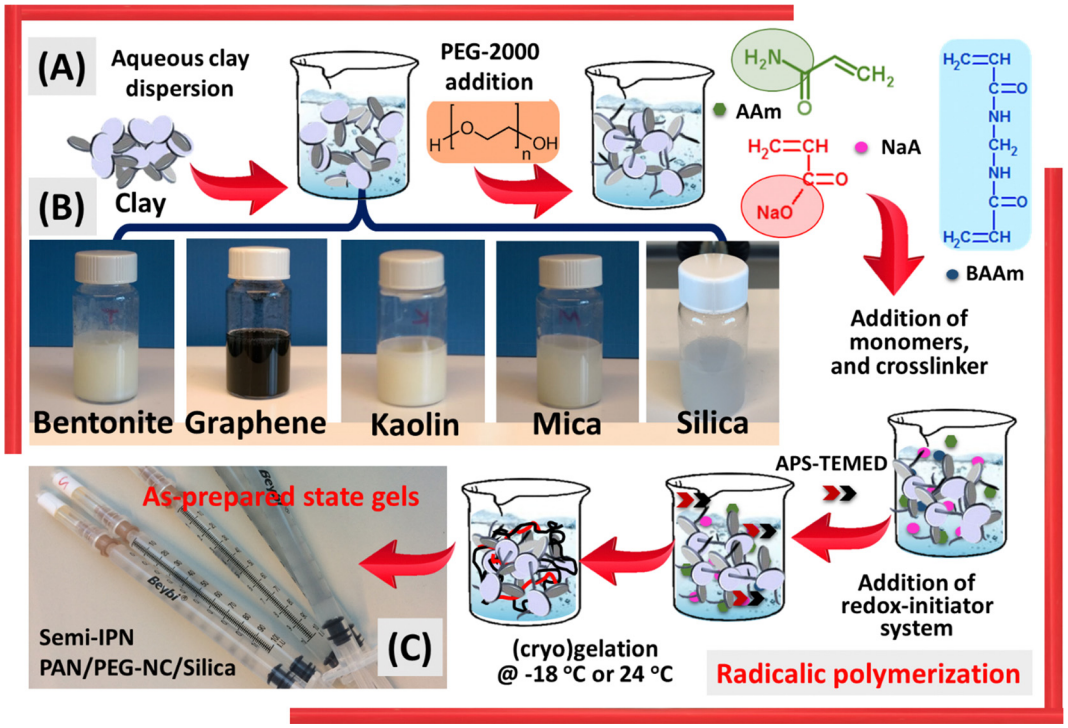

Scheme 1 (A) Synthetic steps performed during preparation of hybrid PAN/PEG-NC gels. (B) Aqueous dispersion of bentonite, graphene, kaolin, mica and silica. (C) Polypropylene syringes containing silica-filled hybrid gels after completion of the polymerization reaction.

NaA, and NC is used to indicate the presence of nanocomponent. The nomenclature PAN/PEG-NC/Bnt refers to the hybrid gels prepared in the presence of Bnt nanoclay. Scheme 1 illustrates the synthetic steps performed during preparation of hybrid PAN/PEG-NC gels as well as hybrid PAN/PEG-NC/Mica hydrogel after preparation state.

Swelling testing of hybrid PAN/PEG-NC gels-doped with different fillers

After polymerization was completed within 48 h, the rod-shaped gels were removed from the syringes and divided into three groups. Scheme 2 presents the optical appearances of as-prepared state hybrid PAN/PEG-NC hydrogels containing various fillers. The gels in the first group were weighed and placed in pure water to be used as the characterization group. The second group of the gels was used in the mechanical measurements and both weight and diameter changes were monitored, while the gels in the third group were separated to be used in the swelling experiments. The swelling degree of the prepared blank gel and hybrid gels were determined by following the diameter change of cylindrical samples. After measuring the initial diameters using a calibrated compass, Mitutoyo Digimatic Caliper, Series 500, resolution: 0.01 mm, the gel samples were immersed into distilled water at ambient conditions for defined periods of time. The change in the diameters of the samples was monitored regularly until the thermodynamic equilibrium was achieved. Under normal conditions, in the swelling process of a gel sample, the swelling is uniform in three dimensions, which is defined as isotropic swelling, which refers to an isotropic volume change defined by its apparent swelling. In each case, the samples were run in triplicate, with the equilibrium swelling ratio φ_V calculated by;

$$\varphi_V = \frac{(D/D_0)^3}{\nu_{rel}} = \frac{1}{\nu_{sw}} \quad (1)$$

where D_0 and D are the diameter of the samples before and after the swelling process, ν_{rel} and ν_{sw} are the characteristic parameters used to relate the gel structure to the physicochemical properties such as the swelling, stiffness, and solute transport and named as the crosslinked polymer volume fraction in relaxed state and the volume fraction of the crosslinked polymer chains in the equilibrium swollen-state, respectively. Eqn (1) correlates the synthesis variables and swelling behavior to make predictions of the stiffness and solute diffusivity characteristics of synthetic gels. Using the mass-based method which relies on the knowledge of polymer and solvent densities and the assumption of additive volumes, the crosslinked polymer volume fraction in relaxed state ν_{rel} was experimentally determined by:

$$\nu_{rel} = \left[1 + \frac{(m_0/m_{dry} - 1)\rho_p}{\rho_S}\right]^{-1} \quad (2)$$

where m_0 is the weight of sample as-prepared state and m_d is the weight of dried gel, respectively, ρ_p is the density of PAAm-based gel, 1.286 g mL^{-1}, and ρ_S is the density of water, 1.0 g mL^{-1}. Additionally, the gel fraction w_{gel}, insoluble fraction of the samples, was determined using the dry masses under the same experimental conditions and three specimens were tested

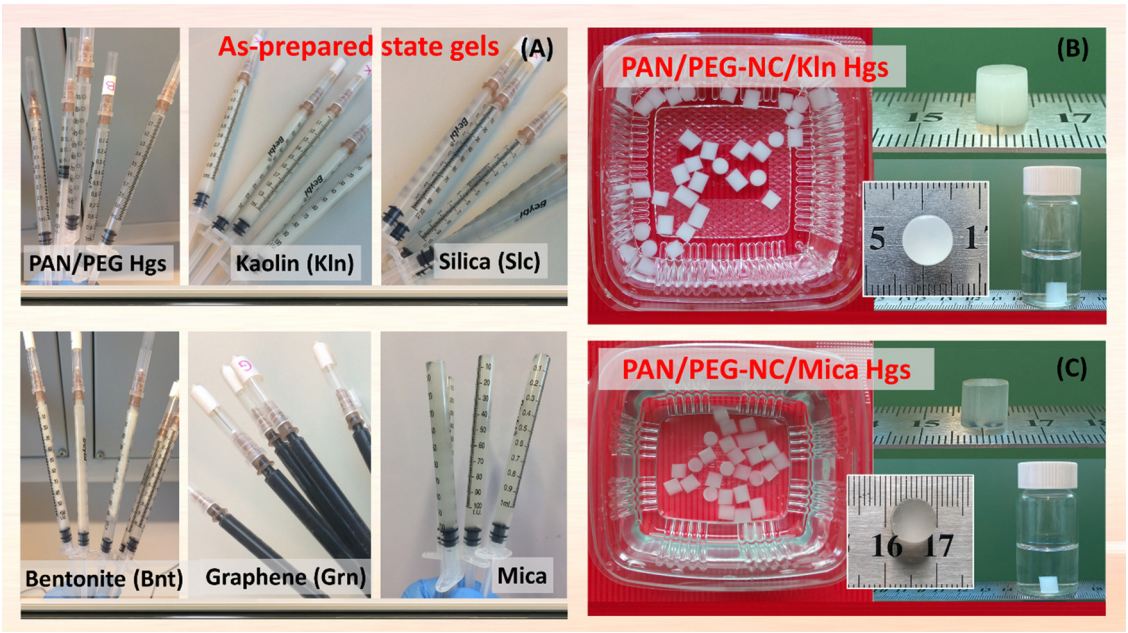

Scheme 2 Optical appearances of hybrid PAN/PEG-NC hydrogels containing various nanofillers after their preparation state (A), swollen-state view of Kln-integrated PAN/PEG-NC/Kln (B) and mica-integrated PAN/PEG-NC/Mica (C) hydrogels after swelling process.

for each synthesis. From the comparative analysis of mass-based determination of polymer volume fractions, the results were presented in Table 1. For hybrid hydrogels, the gel fraction w_{gel} was ranged between 90.4–93.6%, while for the cryogels, it was ranged between 91.2–93.7%. Compared with blank PAN/PEG gels, the addition of various fillers slightly increased the gel fraction of ternary hybrids as the polymer chains growing around the nanoparticles and the aggregation of these particles affected the degree of polymerization. Increasing gel fractions indicate the development of interactions between the layers and polymer chains and confirm the hydrogen-bonded crosslinked structure of hybrids. The network structure of hybrids is tuned by changing the synthesis conditions such as the initial polymer concentration depending on the filler type and the filler–polymer interaction. An opposite trend can be observed with respect to the gel fraction and filler addition, with increasing the filler amount causing an increase in the weight of the gel sample, which may not result in an increased interaction with the gel network and may therefore be associated with the formation of nanoparticle clusters, which will affect the gel fraction to a lesser degree.

Table 1 Physico-chemical network parameters of hybrid PAN/PEG-NC gels. ν_{rel} = the crosslinked polymer volume fraction in relaxed state after preparation, ν_{sw} = volume fraction of crosslinked polymer in the equilibrium swollen-state, and w_{gel} = gel fraction

	Hybrid hydrogels (Hgs)			Hybrid cryogels (Cgs)		
Sample code	ν_{rel}	$\nu_{sw} \times 10^{-1}$	w_{gel}	ν_{rel}	$\nu_{sw} \times 10^{-1}$	w_{gel}
Blank PAN/PEG	0.0530	0.0989	90.4	0.0756	0.2098	91.2
PAN/PEG-NC/Kln	0.0647	0.1048	92.0	0.0704	0.2027	92.4
PAN/PEG-NC/Bnt	0.0612	0.1008	92.2	0.0678	0.1923	92.3
PAN/PEG-NC/Slc	0.0542	0.1173	93.2	0.0501	0.2725	93.7
PAN/PEG-NC/Mica	0.0605	0.1084	93.6	0.0768	0.2195	92.9
PAN/PEG-NC/Grn	0.0594	0.1587	92.5	0.0718	0.5051	93.2

Measurement of point of zero charge (pH_{PZC}) of hybrid gels-doped with different fillers

0.1 M $NaNO_3$ solution (25 mL) was placed in 100 mL Erlenmeyer flasks with the initial pHs ranged between 2 and 12 by the addition of 0.1 M HCl and 0.1 M NaOH in each flask. The initial pH values of the prepared solutions were recorded using a pH meter. Subsequently, approximately 0.10 g of the prepared hybrid gels was added to 25 mL of pH-adjusted solutions in the flasks and shaken at 180 rpm at room temperature for 48 h. After this period, the suspension was centrifuged, and the final pHs of the solution were measured. The ΔpH ($pH_{final} - pH_{initial}$) graph is plotted against the initial pH values and the intersection point of the curves corresponds to the zero charge pH_{PZC} point of the prepared hybrids.

Compressive modulus of hybrid PAN/PEG-NC gels-doped with different fillers

Compressive moduli of hybrids were measured using uniaxial-controlled equipment with a mechanical loading system equipped with a digital comparator (IDC type Digimatic Indicator 543–262, Mitutoyo, Kawasaki, Japan). After measuring the initial sample length L_0, the measurements were conducted between the parallel plates in slow uniaxial compression mode at room temperature to follow the change in the sample length $\Delta L = L_0 - L$, which is the displacement defined as the change in the length relative to the initial length of sample. The uniaxial compression was increased from 0% to 10% in 3 min at a rate of 0.5 mm min^{-1}, while the applied force f was recorded. The relaxation time of network chains was set to 10 s after each

compression and the elastic modulus was determined using the slope of the linear dependence described by the simplified Mooney–Rivlin equation:

$$\sigma = f/S = G(\alpha - \alpha^{-2}) \quad (3)$$

where σ is the nominal stress in Pa m^{-2}, S is the initial cross-section of the sample before measurement, $S = \pi(D_0/2)^2$ and α is the relative deformation ratio of sample as $\alpha = L/L_0$ The geometry of sample is cylindrical, with a diameter of 4–4.5 mm and a height of 5–6 mm. The compressive moduli were obtained as the average values from four experiments.

Study of dye removal capacity of hybrid gels-doped with different fillers

After the prepared hybrids were dried, to analyze their comprehensive performance, the dried samples were ground into fine powder using a mortar and 10 mg of samples was dispersed in 20 mL of MB solution (10–100 mg L^{-1}) and then mixed at 180 rpm using an orbital shaker (Four Es Or-Pro Digital Orbital Shaker) at 23 °C. After adsorbing for a period of time, the swollen samples were filtered, a small amount of the solution was taken and cationic dye MB concentration was determined by UV-vis spectroscopy at λ_{max} of MB 664 nm using the deionized water as a reference. The batch adsorption experiment was performed by agitating the MB solutions at a fixed contact time. The concentrations of MB in the filtrates were determined on the basis of the standard curve of MB using batch equilibration ($A = 0.0443 + 0.1332C$, $R^2 = 0.9990$). Adsorption isotherm was studied for optimization of MB adsorption mechanism and effective design of adsorption. The experimental design was based on three independent factors; type of filler in the structure, initial MB concentration, and contact time at three levels. The results expressing the surface properties and capacities of hybrid gels were evaluated according to the filler types included in the structure. The equilibrium adsorption isotherm was evaluated at constant optimum conditions of the contact time as 24 h, adsorbent dose as 10 mg, and initial MB concentrations varied from 20 to 100 mg L^{-1} (*i.e.*, 20, 40, 60, 80, and 100 mg L^{-1}). Dye adsorption capacity of MB onto hybrid gels at equilibrium, q_e (mg g^{-1}) and at time t, q_t (mg g^{-1}) was calculated using the following equations:

$$q_e = \frac{(C_i - C_e)V}{m} \quad \text{and} \quad q_t = \frac{(C_i - C_t)V}{m} \quad (4)$$

where C_i is the initial concentration of dye (mg L^{-1}), C_e and C_t are the concentration of MB dye at equilibrium and at time t (mg L^{-1}), respectively. V is volume of the dye solution (L), and m is the mass of dry adsorbent (g). The adsorption% of MB dye by hybrids was determined using the following equation;

$$\text{Adsorption } (\%) = \frac{(C_i - C_t)}{C_i} \times 100 \quad (5)$$

Based on the adsorption kinetics, to analyze the cationic MB adsorption of nanofiller-integrated hybrid gels, pseudo first-order (PFO), pseudo second-order (PSO), Elovich, intraparticle diffusion model and Avrami kinetic models were tested. For the adsorption isotherm analysis, the data were simulated using five isotherm models including Langmuir, Freundlich, Redlich–Peterson, Sips, and Dubinin–Radushkevich (D–R) model.

Characterization of hybrid PAN/PEG-NC gels-doped with different fillers

ATR-FTIR spectra were conducted on a with a PerkinElmer Spectrum 100 FTIR in the attenuated total reflectance mode at a resolution of 4 cm^{-1} in a scanning range of 600–4000 cm^{-1}. XRD patterns were performed on a Bruker D8 Advance X-ray diffractometer in the region of diffraction angle (2θ) from 4° to 50° with Cu-Kα radiation at λ = 0.154 nm. By applying an accelerating voltage of 40 kV and a current intensity of 40 mA, the scans were detected with an angular step of 0.02°. Thermodegradation analysis was carried out on a SEIKO EXSTAR 6200 Model TG/DTA thermogravimetric analyzer using dry nitrogen purge at a heating rate of 10 °C min^{-1}. The measurements were detected in the temperature range of 25–600 °C at a speed of 150 mL min^{-1} under a nitrogen atmosphere. For the adsorption measurements of MB dye, a UV-vis spectrophotometer (Novel N4S UV-vis spectrophotometer) with a wavelength range 190–1100 nm and wavelength repeatability $\leq$0.5 nm was used. For the measurements, the photometric accuracy was $\pm$0.3%T with $\pm$0.002 Abs (0–0.5 A) and photometric repeatability $\leq$0.15%T. For adsorption data analysis, UV WIN8 Spectrum data processing software was used. During the adsorption tests, an orbital shaker (Four Es Or-Pro Digital Orbital Shaker) with a 32 × 32 cm universal holder table was used to continuously shake the samples, operating at 20–500 rpm.

Results and discussion

The aim of this study is to improve the performance of ternary polyacrylamide-based gels by utilizing novel linking methods in which various organic and inorganic components are integrated to form multifunctional hybrid networks. Based on this hypothesis, comprehensive insights into the structural and compressive modulus changes of anionic copolymer gel formed in the presence of linear PEG chains by the integration of various fillers have been provided. These changes were visualized and quantified by a range of analytical techniques, while both the immediate and recovery responses and mechanical properties of ternary hybrid networks were evaluated according to the type of nanoparticles incorporated into the structure.

Effect of filler incorporation on structure of hybrid gels

To evaluate polymer–filler interactions, Fig. 1 presents ATR-FTIR spectra of the raw nanofillers and their hybrid counterparts. The spectrum of the blank PAN/PEG hydrogel is included for comparison, highlighting the interactions between the fillers and the polymer network to make the role of fillers in the nanocomposites more apparent and to strengthen the overall argument. The spectrum of blank PAN/PEG hydrogel is composed of bands from AAm, anionic comonomer NaA and

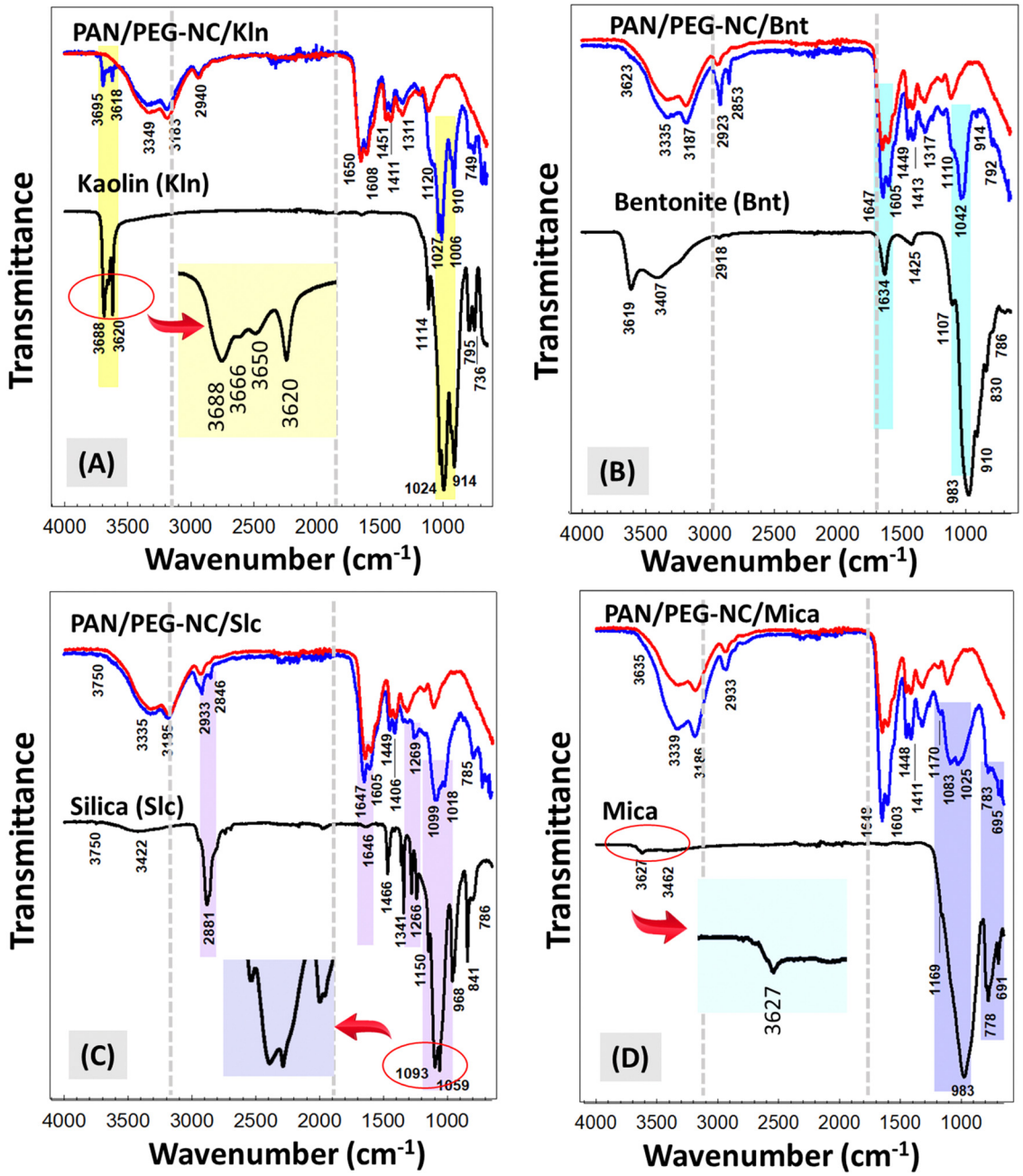

Fig. 1 ATR-FTIR spectra of raw Kln, hybrid PAN/PEG-NC/Kln (A), raw Bnt and hybrid PAN/PEG-NC/Bnt (B), raw Slc and hybrid PAN/PEG-NC/Slc (C), raw Mica and hybrid PAN/PEG-NC/Mica (D). The red lines correspond to the spectrum of blank PAN/PEG gel for comparison.

PEG moieties. The asymmetrical and symmetrical stretching vibration peak of $-NH_2$ groups on PAAm moiety were detected at 3354 cm^{-1} and 3178 cm^{-1}, respectively.[16] N–H stretching of PAAm units seen at around 3350 and 3190 cm^{-1} was observed all the hybrid hydrogel samples with a slight shift. Asymmetric C–H stretching vibrations placed in the groups of polymer alkyl chains and cross-linking points were detected at about 2938 cm^{-1}. The characteristic peaks at 1653, 1602 and 1448 cm^{-1} were attributed to the stretching vibration of carbonyl group (C═O), the bending vibration of N–H of amide groups, and the C–N stretching on PAAm chains, respectively.[17] The bands at 1560 and 1405–1410 cm^{-1} were due to the asymmetric and asymmetric stretching mode of carboxylate (COO^-) group of NaA units, respectively. The stretching vibrations of carboxylate of NaA units and C–N from PAAm units are superposed at 1405–1411 cm^{-1}.[18] In the fingerprint area, small shifts of the doublet at 1450 and 1420 cm^{-1} were observed for the hybrid gels. The band at 1324 cm^{-1} corresponding to –C–N– group of cross-linker BAAm forming cross-bridge bonds between the network chains was detected in the spectra of all gel samples.[19] The peak appeared at 1178 cm^{-1} was considered due to the stretching vibration of –CO–O– group of NaA units.[20] The absorption

peak at 2858 cm^{-1} was corresponded to the stretching modes of CH_2 in PEG while the strong absorption peak of C–O, and C–C stretching of PEG moiety was detected at 1120 cm^{-1} indicating the presence of PEG chains in the copolymer poly(acrylamide-*co*-sodium acrylate) matrix.[21]

In Fig. 1(A), the characteristic absorption peaks of Kln observed at 3688 and 3620 cm^{-1} were assigned to the in-phase vibration of the inner surface hydroxyl and inner hydroxyl, respectively.[22] Four types of hydroxyl groups have been identified in kaolinite: external surface hydroxyl, internal surface hydroxyl, internal hydroxyl and absorbed water hydroxyl.[23] As shown in the inner part in Fig. 1(A), the bands at 3666 and 3650 cm^{-1} belong to the characteristic vibration bands of outer surface hydroxyl and absorbed water. In the spectrum of the PAN/PEG-NC/Kln hybrid, the observation of these bands at 3695, 3669, 3652 and 3618 cm^{-1} supports the successful incorporation of Kln into the semi-IPN structure.[23] A significant decrease in the intensity of the bands at 3695 and 3618 cm^{-1} of Kln was observed, while the characteristic peaks of the inner surface O–H group shifted from 3688 to 3695 cm^{-1}, indicating that the interaction between –OH groups on Kln and hybrid chains occurred during the polymerization.[24] For poly(acrylic acid-*co*-acrylamide)/Kaolin composites, similar observation was reported by Liang and Liu.[25] For raw Kln, the peak at 914 cm^{-1} was due to bending vibration of (Al)O–H. The main Kln peaks were detected at 1024 and 795 cm^{-1} which are the Si–O stretching and Si–O–Si stretching frequencies, respectively. The peaks observed at 1114, and 736 cm^{-1} were attributed to the interference of clay minerals like quarts and muscovite. The absorption peaks of Kln exist at 1027 and 910 cm^{-1} in the spectrum of PAN/PEG-NC/Kln hydrogel, which provides evidence that the Kln acted as a physical filler in the hybrid network.[26] The FTIR spectrum of raw Bnt was given in Fig. 1(B). The characteristic vibrations of raw Bnt observed in the region of 910–1110 cm^{-1} were assigned to Si–O–Si, Al–O and Si–O stretching vibrations, and additional bands between 786 and 830 cm^{-1}, were assigned to Al–OH–Mg bonds and Fe^{3+}–OH–Mg bonds, respectively.[27] The peak at 3619 cm^{-1} was attributed to Al_2OH stretching, while the broad peak at 3407 cm^{-1} belongs to the OH stretching of H-bonded water of raw Bnt, which is reported to be intensified due to more octahedral Mg atom substitution than Fe atoms.[28] In the spectrum of hybrid PAN/PEG-NC/Bnt gel, the slight peak at 3623 cm^{-1} was detected due to the interaction between Bnt and hybrid network. The peak assigned to the OH deformational mode of water was observed at 1634 cm^{-1}, while the peak at 1107 cm^{-1} was due to the longitudinal Si–O stretching mode.

The Si–O–Si stretching peaks of tetrahedral layer was clearly observed at 983 cm^{-1}, while the OH bending peaks of octahedral layer was detected at 910 and 830 cm^{-1}, respectively.[29] The peak at 786 cm^{-1} originates from the external clay component quartz, while the peak occurred at 1425 cm^{-1} was due to the presence of calcite. The main characteristic bands identified in both Bnt and PAN/PEG gel were observed in PAN/PEG-NC/Bnt spectrum, confirming the interactions between Bnt and the hybrid network. A band in the range of 1110–1042 cm^{-1}, which increased with the incorporation of Bnt and shifted towards larger wave numbers, was attributed to the Si–O–Si stretching vibrations originating from Bnt.[30] The spectrum of raw Slc, Fig. 1(C), showed a broad band in the range of 3000–3800 cm^{-1} with a maximum at 3422 cm^{-1} assigned to OH bond stretching of the surface silanol groups.[31] The peak of 3750 cm^{-1} was due to isolated silanol vibrations[32] while the symmetric mode of Si–O–Si band was detected at 786 cm^{-1}.[33,34] The stretching vibration of Si–O was observed between 968 cm^{-1} and the band at 1646 cm^{-1} represents the terminal silanol groups Si–OH which is responsible for the adsorption of water molecules, while the C–H stretching vibration appeared at 2881 cm^{-1}. The discrete sharp band at 841 cm^{-1} was ascribed to O–H bending mode of hydrogen bonded, while the Si–O in-plane stretching vibrations of the silanol Si–OH groups observed at 968 cm^{-1}. The sharp band appearing at 1093–1059 cm^{-1} and the shoulder at around 1150 cm^{-1} were attributed, respectively to the transversal optical and longitudinal optical modes of the Si–O–Si asymmetric stretching vibrations. This band was shifted towards higher wave number at 1099 and 1018 cm^{-1} in PAN/PEG-NC/Slc Hgs.[33] Similarly, the peak at 1266 cm^{-1} corresponding to Si–O stretching was shifted towards the higher wavenumber, 1266 cm^{-1} in PAN/PEG-NC/Slc Hgs.[34,35]

In Fig. 1(D), the absorption bands of mica found at 3621 cm^{-1} was attributed to the Si–OH stretching vibration close to neighboring octahedral sites filled with divalent ions; Fe^{2+} and Mg^{2+}, the characteristic absorption band at 3462 cm^{-1} showed asymmetrical stretching vibration of –OH groups.[36] The strong absorption band at 983 cm^{-1} represented Si–O–Si stretching vibration of mica.[37] Hybrid PAN/PEG-NC/Mica sample displayed two discrete sharp bands at 1083 and 1025 cm^{-1} presumably due to N–H stretching vibrations and out-of-plane stretching vibration of Si–O–Si, respectively. The results showed successful loading of mica into the hybrid gel structure. Moreover, the sharp peak at 778 cm^{-1} is due to the Al–O stretching vibration of mica, while the shift of this peak towards higher wavenumber at 783 cm^{-1} in the hybrid structure is the result of the interaction between mica and the hybrid network. The rather sharp band at 691 cm^{-1} was attributed to Si–O stretching vibration coupled with Mg–O vibration. Similarly, the peak at 691 cm^{-1} shifted towards the higher wave number, 695 cm^{-1}, for the hybrid gel corresponding to the Si–O bending with Mg^{2+} ions, indicating that the overall structure of mica was preserved in the hybrid gels.[38,39] All these observations indicated that clay particles were present in the structure of the ternary hybrid gels. Similar obervations reported by Ibraeva and coworkers for organic–inorganic hybrid composites consisting of PAAm and clay minerals such as bentonite, montmorillonite, kaolin as well as silica and titanium dioxides designed by *in situ* synthetic protocol. FTIR and Raman spectroscopy results revealed formation of hydrogen bonds between NH_2 groups of PAAm and oxygen groups of TiO_2, SiO_2 and aluminosilicates.[40]

Fig. 2 shows TG curves of raw fillers and hybrid PAN/PEG-NC hydrogels. Table S3 (ESI†) present the data showing % mass loss of raw fillers at temperatures 120 °C and 800 °C. As seen in TG curve of raw Bnt, 14.0 wt% of water was liberated below

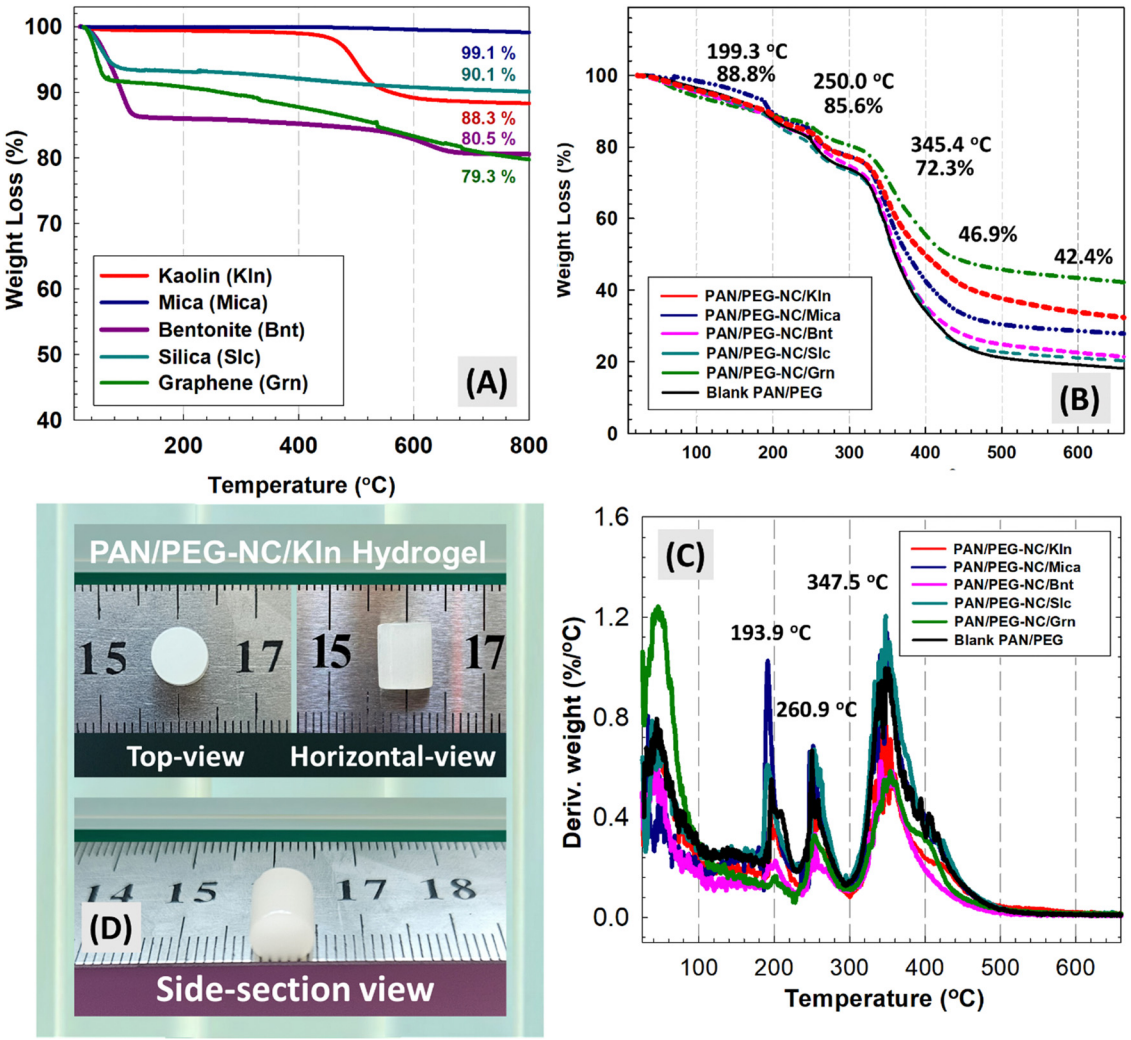

Fig. 2 TG curves of raw fillers (A), TGA (B) and DTG (C) curves of hybrid PAN/PEG-NC hydrogels. The weight loss and corresponding temperature data for blank PAN/PEG hydrogel were indicated. (D) Optical view of Kln-integrated hybrid PAN/PEG-NC/Kln gel sample from different perspectives regarding the gel homogeneity.

158 °C, and the water loss was not rapid until about 591.7 °C (83.1 wt%). Between 522.6 and 650.2 °C, a second slight reaction occurred with a percent mass loss of 4.9 wt%. In the range of 650–800 °C, Bnt nanoclay was stable and the percent mass loss, 80.5 wt%, was constant.[41] Thermogram of raw kaolin showed a two-step weight loss; only small amount of water liberation below 140 °C was due to the evaporation of adsorbed water. In the second step between 464–541 °C, the weight loss 11.6 wt% was assigned to dehydroxylation of kaolin and formation of metakaolin ($Al_2Si_2O_7$). With heating up to 800 °C, due to removal of zeolitic water raw kaolin showed a mass loss of 11.7 wt%.[42] Mica was almost stable and displayed no mass loss all over the temperature range. Only above 300 °C, it begun to lose small amount of water. The loss of water was not rapid, and at 800 °C, the mass loss was 0.9 wt%.[43] Slc nanoparticles had a single degradation stage at 26.9 °C with a weight loss of 0.2 wt%, which was the loss of the moisture retained in the Slc nanoparticles. Above this initial stage, Slc was almost stable and at 800 °C, the mass loss was 0.9 wt%. Grn showed about 8.3 wt% mass loss below 100 °C resulting from the evaporation of adsorbed water. The thermal stability started to decrease at a temperature of about 100 °C which can be associated with structural rearrangement of carbon and displayed a gradual mass loss due to the disruption of the carbon network.

Blank PAN/PEG hydrogel indicated three-stages of thermal decomposition: 174.3–225.2 °C, 222.5–289.6 °C and 289.6–441.3 °C. The second stage was related to the depolymerization reactions and intermolecular dehydration reactions; with a weight loss of approximately 17.1%. The third stage of decomposition was attributed to the main chain degradation of copolymer and PEG units with a weight loss of approximately 26%. To gain more insight into the formation of hybrids and to determine the rate of degradation, TGA curves of representative PAN/PEG-NC hydrogel incorporated with 1.50% (w/v) of various fillers were compared in Fig. 2. For all samples, minor weight

loss was observed at temperatures less than 200 °C which is associated with the loss of adsorbed water on the surface of the particles known as bound water. Most of these hybrid gels exhibited a three-stage thermal decomposition except for that of incorporated with Grn nanosheets, which exhibited a two-stage decomposition. Although derivative weight loss curve of Grn-loaded hybrid gels showed a broad peak with a maximum at about 199.3 °C, it was assumed to be two-stage degradation which may be attributed to the structure difference of Grn nanosheets comparing with other clays. Following the initial stage within the temperature of 174.9–222.5 °C, there was weight loss of 19.2% between 222.5 and 293.2 °C assigned to the thermal decomposition of amide side groups of AAm and crosslinker on the network. Beyond 294 °C up to 471.3 °C, the weight loss was 53.1% as a result of depolymerization reactions and the breaking of the crosslinks between the polymer chains.

The maximum thermal decomposition temperatures, corresponding mass loss, and char yield of the samples were shown in Table S4 (ESI†). The char residue at 650 °C and thermal stability of hybrid PAN/PEG-NC samples incorporated with the same content of nanofillers is in the order Grn > Kln > Mica > Bnt > Slc > PAN/PEG. TG curves showed that once the thermally resistant fillers were incorporated, the thermal motion of polymer chains within hybrid gels was consequently impeded, thereby enhancing the thermal stabilities of the hybrids and Grn nanosheets could enhance the thermal stability to the highest degree among the nanofillers investigated. These results are supported by the XRD spectra obtained for the Grn-doped PAN/PEG-NC/Grn gels. The weight loss trends appear to be different between nanofillers and hybrid PAN/PEG-NC samples. Bare mica shows almost no weight change when heated, but hybrid PAN/PEG-NC/Mica sample exhibits significant weight loss. In contrast, bare Grn experiences significant weight loss when heated, but the hybrid PAN/PEG-NC/Grn sample exhibits minimal weight change. Souza and coworkers reported that inclusion of mica at different composition may lead to a significant decrease in T_g by a plasticizing effect and to promote the speed up of crystallization and therefore, an increase in the crystallization rate of poly(lactic acid), which may reduce thermal stability.[44] When comparing the nanofillers, the 42.2% residue is based on the fact that while Grn as a filler maintains a good dispersibility in the polymer matrix, the char retention is high. The excellent reinforcements were attributed to good dispersion of Grn and strong interfacial adhesion between layered stacks of Grn nanosheets and semi-IPN PAN/PEG matrix which is well consistent with the previous report of Akinyi *et al.* for hybrid graphene–clay/polyimide nanocomposites. It was reported that at higher Grn loadings, poor dispersibility occurs and therefore the thermal decomposition and stability of hybrid are affected.[45] The higher improvement in the stability of the matrix was attributed to the homogeneous distribution of Grn nanosheets being more conducive to improving the thermal stability. Moreover, Grn nanosheets act as barriers to prevent oxygen permeation and volatile degradation products escape, thus promoting charring, so-called ''tortuous path'' effect.[46] The chemical structure of fillers and their state existed in the hybrid network may be the main reasons for the observed difference in TG results of hybrid PAN/PEG-NC gels.

Fig. 3(A) shows XRD pattern of bare Slc and Slc-integrated PAN/PEG-NC/Slc gel comparing with blank PAN/PEG gel. The bare Slc spectrum showed a broad peak with a Bragg angle at $2\theta = 22.4^\circ$, which is the characteristic peak of amorphous Slc particles.[47] The blank PAN/PEG gel showed a broad peak with a maximum at $2\theta = 14.5^\circ$, which was also observed at 14.6° after integrating Slc nanoparticles into PAN/PEG-NC/Slc. The hybrid gel showed a maximum at 23.5°, which is attributed to the presence of extensive hydrogen bonding between the silanol of Slc and the carbonyls of PAN/PEG network.[48] XRD patterns of raw Kln and PAN/PEG-NC/Kln hybrid gel were presented in Fig. 3(B). The raw Kln showed strong diffraction peaks at $2\theta = 12.3^\circ$ and 24.9°. The other peaks detected for Kln at 17.76°, 20.85°, and 26.64° showed the existence of crystalline phases namely; quartz hexagonal, kaolinite triclinic, montmorillonite hexagonal, koenite hexagonal and potassium silicon hydride cubic.[49] In the Kln-integrated PAN/PEG-NC/Kln gel, the characteristic peaks of Kln nanoclay are observed at the same angles, confirming the incorporation of Kln into PAN/PEG matrix to form hybrid structure. The reflection corresponding to d_{001}-value of Kln was observed in PAN/PEG-NC/Kln sample which seems to indicate that the acrylamide polymerization in the presence of sodium acrylate and PEG chains led to disordered Kln structures in the hybrid matrix. Kln showed enhanced interactions between the filler and the PAN/PEG matrix, through the interactions between amino ($-NH_2$) from PAAm and carboxylic groups (–COOH) from sodium acrylate and hydroxyl of PEG chains. Similar results have been reported by Zaharia and coworkers for nanocomposites based on the cross-linked poly(acrylic acid) and kaolinite, modified with different loadings of PAAm prepared by inverse dispersion polymerization.[50] The obtained results showed that acrylic acid polymerization led to the formation of exfoliated/disordered kaolinite and especially the PAAm modified surface of kaolinite led to an increase in the interlayer space, facilitating the penetration of acrylic acid and its polymerization into the interlayer space of kaolinite layers, thus leading to the formation of nanocomposite structures.

From Fig. 3(C), it is observed that the raw Bnt contains sodium-rich montmorillonite as the dominant clay mineral with a characteristic diffraction peak at $2\theta = 6.6^\circ$ corresponding to the interlayer distance (d-space) of 13.30 Å. Other characteristic peaks at $2\theta = 19.7^\circ$ and 34.9° with d values of 4.48 Å and 2.57 Å indicated that montmorillonite appears well crystallized in the sample. The peak at $2\theta = 28.5^\circ$ was corresponded to quartz impurity in Bnt.[51] While the main diffraction peak of Bnt is observed at the same 6.6° angle, the large decrease in the peak intensity in hybrid PAN/PEG-NC/Bnt gel indicates the interaction between Bnt nanoclay and PAN/PEG chains. Similar results were observed by Khan and coworkers and in the diffractogram of PAAm/bentonite hydrogel nanocomposite, the disappearance of the basal peak of bentonite was stated to depict the exfoliation phenomenon, while the decrease in the

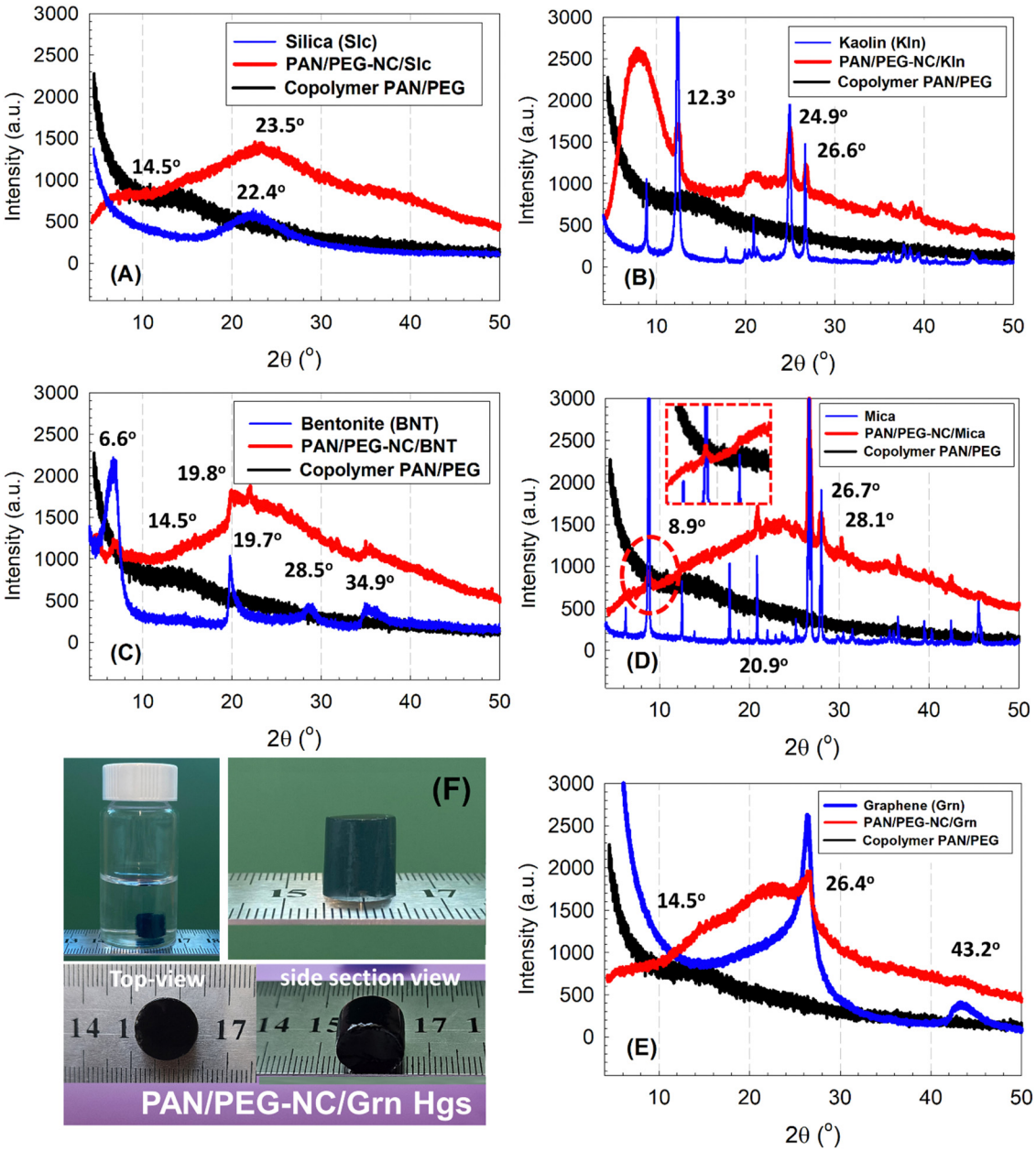

Fig. 3 XRD patterns of hybrid PAN/PEG-NC integrated with Slc (A), Kln (B), Bnt (C), Mica (D) and Grn (E). Optical views of swollen state Grn-doped PAN/PEG-NC/Grn gels from different perspectives (F).

intensity of some crystalline peaks confirmed the polymerization of AAm.[52] After the interaction between Bnt and PAN/PEG polymeric matrix, the peak of montmorillonite (2θ = 34.9°) was also preserved.[53] Similar results were reported by Wali and coworkers for Bnt-grafted poly(acrylamide-*co*-acrylic acid) superabsorbent composites, and it was suggested that interlayer penetration may occur in the acrylamide and acrylic acid solution.[54]

In Fig. 3(D), XRD pattern of bare mica showed a strong peak at 2θ = 8.9° corresponding basal plane of (003) with a basal spacing of 9.92 Å. The peaks detected in the spectrum at 2θ = 6.2°, 12.5°, 17.9, 36.5°, 39.5°, and 45.5° were due to the polycrystalline structure mica as well as the presence of the other silicates; chlorite and quartz.[55] In the XRD pattern of hybrid PAN/PEG-NC/Mica, the presence of the peak at 2θ = 8.6° observed with low intensity indicates the presence of mica in the hybrid structure. The other characteristic peak of mica was detected at 2θ = 20.9°, 26.7°, and 28.1° in hybrid gels. In their work on fabricating Mica/poly(acrylic acid) nanocomposites, Lin and coworkers reported that the synthesis of nanocomposites consisting of polymer and ultrafine mica particles, by grafting acrylic acid polymer onto mica, is mainly based on the reaction between the OH groups on the mica surface and the COOH groups on the acrylic acid.[56] Unlike this method, in

which pure mica is incorporated into poly(acrylic acid) to prepare nanocomposites, in the synthesis proposed by Lee and Chen, reactive mica was prepared by intercalating hydrophilic vinyl monomer into mica in the first step, and then polymerization was carried out in the interlayer galleries of mica.[57] It was stated that no reaction took place between OH groups on the mica surface and COONa groups on sodium acrylate, suggesting that mica did not act as an additional network point and pure mica did not increase the cross-link density of the composite gel. Therefore, it was concluded that this method is important for improving the water-absorbing properties of superabsorbent materials. In Fig. 3(E), the observed peaks in XRD pattern confirmed the crystalline nature of the raw Grn. A sharp intensive peak observed at 2θ of 26.4° corresponding intense (002) plane is highly specific for the crystalline nature of Grn samples. XRD pattern showed additional peak at 2θ value of 43.2° for the 101 plane. Similar results were reported by Selvam and coworkers for graphene sheets obtained through the reduction of graphene oxide from hydrazine hydrate.[58] The diffractogram of Grn-doped PAN/PEG-NC/Grn gel showed an amorphous structure of the cross-linked hybrid matrix compared to blank PAN/PEG, while the peak observed at 26.4° corresponding to the (002) reflection of Grn nanosheets indicated the partial rearrangement, which is based towards the presence of Grn in the structure. The dispersion level of nanofiller in the semi-IPN matrix and the interfacial interaction between the nanofiller and PAN/PEG matrix are two decisive factors to affect the properties improvement of hybrid samples. The broad peaks observed at 26.4° and 43.2°, indicated disordered graphene nanosheets dispersed in the matrix. XRD results proved the formation of hybrid gels with significant structural changes upon different types of filler doping.

Effect of filler incorporation on elasticity of ternary hybrid gels

The mechanical properties of PAN/PEG gels were changed by altering the filler-type incorporated into the ternary structure. The cross-link density was estimated for hybrid PAN/PEG-NC gels with different fillers. The effects of filler-type and the polymerization temperature on the mechanical properties were discussed on the basis of the network structure of hybrids. Upon completion of the gelation at ambient temperature, the hybrid hydrogels were subjected to the uniaxial compression testing and the results were collected in Fig. S1(A) (ESI†). Due to the presence of frozen parts in the synthesis carried out at −18 °C, the syringes were first brought to room temperature and the gels were removed from the syringe and swollen in water, and then, the mechanical measurements were performed in the swollen state.

The swollen-state measurements of hybrid hydrogels and cryogels were presented in Fig. S1(B) and (C) (ESI†). Based on the simplified Mooney–Rivlin equation given by eqn (3), the compressive elastic modulus of hybrid gels after-preparation-state and after swelling-state were determined from the slope of stress–strain curves in Fig. S1 (ESI†) and the results were collected in Fig. 4(A). The elastic moduli of hybrid hydrogel and cryogels incorporated with the same content of inorganic component is in the order NC-Grn > NC-Slc > NC-Mica > NC-Kln > NC-Bnt. Graphene-doped hybrid PAN/PEG-NC/Grn gels exhibited the highest G_0 and G values with the lowest swelling degree, while Bnt-doped gels had the lowest elastic modulus. The results were attributed to the presence and fine dispersion of Grn nanosheets consisting of short stacks of platelet-shaped sheets that are in a planar form. Kln and mica are non-swelling 1 : 1 and 2 : 1 minerals, respectively, while Bnt is a swelling 2 : 1 mineral but has different interlayer cations and layer charges.[17] Ding and coworkers studied the elastic properties of polyacrylamide hydrogel enhanced by kaolinite with a highly exposed layer surface by the intercalation–expansion method with a crosslinker function.[59] Kaolinite shows a lamellar aggregate morphology with the accumulation of hydrogen-bonded aluminosilicate layers, while most of the hydroxyl groups with reactive functions are hidden within the tightly packed aluminosilicate layers. In the hydrogel system, the kaolinite layer acted as an additional crosslinker by promoting the formation of a complex crosslinking network with the participation of surface hydroxyl groups. The surface functional groups reacted with the polyacrylamide molecular chains, increasing the flexibility of the matrix. With the addition of Grn nanosheets, a 4.1-fold increase in the post-synthesis modulus of PAN/PEG hydrogel was observed, while with the addition of Slc, the increase was 3.3-fold. Due to the strong surface activity of hydrogen groups on the surface, Slc particles were distributed on the surface of PAN/PEG network and strongly bonded to the network chains, strengthening the interface interaction between these two components. Wu and coworkers studied the effects of Slc content (varied between 0 and 10% in relation to the whole system) on the properties of polyacrylamide/Slc composite hydrogels prepared *via in situ* free-radical polymerization.[60] When the Slc content was 15%, the maximum elastic modulus was 16.1 kPa, and adding more Slc to the network structure increased the amount of energy required for fracture under compression. Slc nanoparticles stiffens the network by creating additional physical crosslinking points, while the brittle nature of the bonds and the wide distribution of distances between crosslinks can create a wide dissipative zone. For poly(dimethylacrylamide)/Slc hybrid hydrogels, Lin and coworkers reported that adsorption of poly(dimethylacrylamide) chains onto Slc nanoparticles results in the formation of a physical network due to the presence of hydroxyl groups. Chemically cross-linked gels containing polymers physically adsorbed onto Slc nanoparticles provide a common way to improve the properties. Both physical adsorption and the presence of chemical covalent bonds are important in determining the mechanical properties in filled rubber architectures.[61] Based on Rubber elasticity theory, the compressive modulus as-prepared state G_0 relates with the crosslinking density ν_e by:

$$G_0 = A\nu_e RT\nu_{rel} = A\frac{RT}{NV_1}\nu_{rel} \quad (6)$$

which characterizes the elasticity of as-prepared state real network as a function of the polymer concentration. To determine

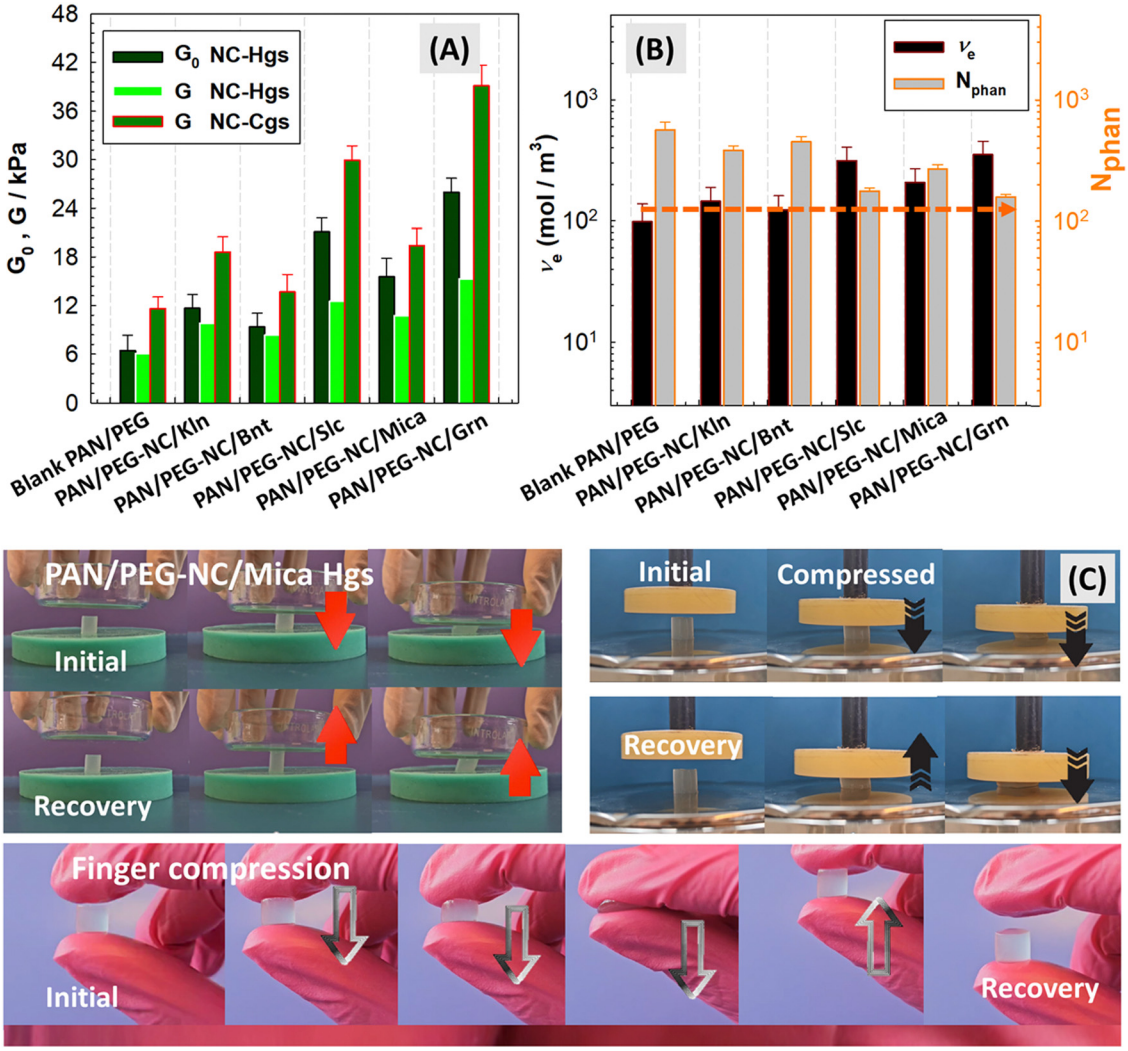

Fig. 4 (A) Comparison of compressive elastic moduli at equilibrium swollen state G with that of as-prepared state G_0. (B) Effective crosslink density and network chain length N of hybrid PAN/PEG-NC gels calculated by phantom network model. (C) Optical views of mica-doped hybrid gels during uniaxial compression and finger testing; before and after removal of stress.

the structural relationship between the compression modulus and mesh size of hybrid gels, both the effective crosslink density and mesh size were estimated for each hybrid formulation using model eqn (7), and the results are shown in Fig. 4(B) according to the filler type. As seen in Fig. 4(B), Slc nanoparticles reduced the chain length between two cross-linking points in the gel structure the most compared to the blank PAN/PEG gel due to the formation of Slc-filled hybrid network and physical cross-linker.

Fig. 4 presents the optical views of mica-doped hybrid gels during uniaxial compression and finger testing; before and after removal of stress. Fig. S2 and S3 (ESI†) show the behavior of Slc, Bnt, Grn and Kln-integrated hybrid samples during the uniaxial compression and manual compression. When compared to Slc-doped hybrid gels, it is seen that the crosslink density in mica-doped hybrid gels is higher than in PAN/PEG gels. For the composites of polypropylene with mica powder produced by melt mixing, Khonakdar and coworkers reported that treated mica increases the flexural modulus, with the result that the impact strength of the composites decreases with increasing mica concentration. Treated or untreated mica has been reported to act as a stress concentrator.[62] In another work, Wan and coworkers prepared microcrystal muscovite composites by water solution polymerization using acrylic acid, acrylamide and itaconic acid as comonomers.[63] The increase in the gel strength can be attributed to the increase in the cross-linking points, as the OH groups in the microcrystalline muscovite structure act as physical crosslinks. When the amount of muscovite exceeds 15%, the gel strength decreases as the presence of excessive particles reduces the polymerization rate and the free volume of the polymer matrix.

Effect of filler incorporation on swelling of hybrid gels

The swelling of hybrid gels based on anionic polymer matrix and inorganic nanofillers varied depending on the filler-type and their distribution in the hybrid matrix (Fig. 5). The lower molecular flexibility of ternary hybrid structure, with fillers having surface functional groups acting as an additional

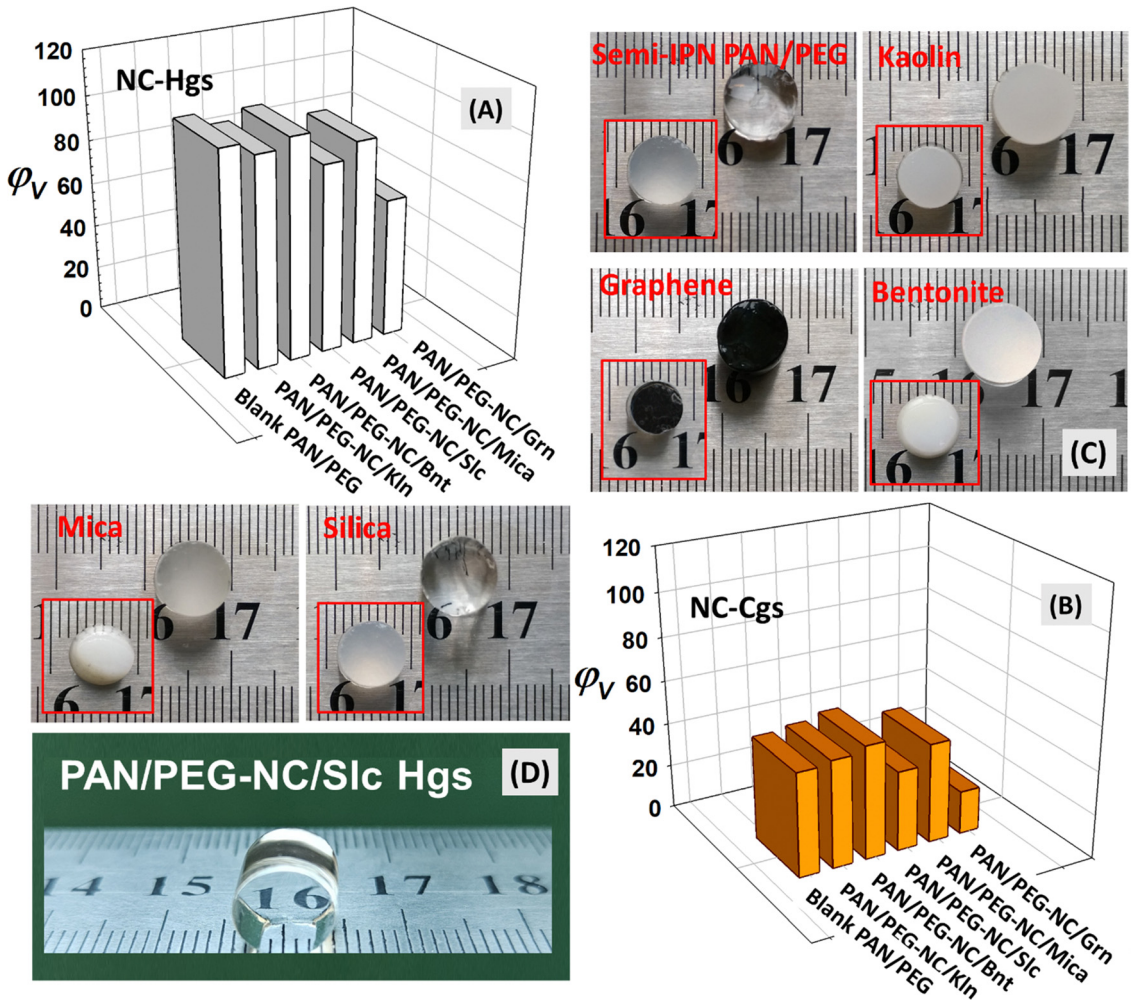

Fig. 5 The equilibrium volume swelling ratio of hybrid PAN/PEG-NC Hgs (A) and that of Cgs (B). Comparison of the optical appearances of semi-IPN PAN/PEG, Kln, Grn and Bnt-doped hybrid hydrogels (C) and mica and Slc-doped hybrid hydrogels (D) after reaching swelling equilibrium with the cryogels shown in the red frame.

crosslinking agent, reduced the water absorption. The blank PAN/PEG hydrogel without filler and Slc-integrated PAN/PEG-NC/Slc hydrogel was highly transparent, while Grn-doped gels are black in color, and all cryogel samples are opaque in color, with varying brightness. Considering the presence of 5.14% (w/v) PEG in the copolymer structure, both blank PAN/PEG Hgs and Cgs showed high swelling capacity due to the hydrophilic nature of PEG. The ether groups in PEG are hydrophilic and in aqueous solution PEG tends to bind two or three water molecules per ethylene oxide unit, leading to a large exclusion volume. For the present hybrid system, the equilibrium water absorbency of hybrid gels incorporated with the same amount of nanofiller is in the order NC-Bnt > NC-Kln > NC-Mica > NC-Slc > NC-Grn. Among the nanofillers used, Bnt nanoclay can form multiple water layers in the interlayer space, potentially affecting swelling giving hybrid gel network enough space to absorb and hold the water molecules. The relatively high swelling capacity of hybrid hydrogels and cryogels-doped with Kln and Bnt nanoclays is due to the higher specific surface area of Bnt compared to Kln, which causes more swelling. The weakening of electrostatic interactions due to the screening of the surface charge by the binding of polymer chains to the negatively charged Bnt surface and the attraction of water molecules by the network chains along the diffusion gradient dominates the swelling. In studies examining the different effects of Bnt and Kln on composite hydrogels, it was reported that Kln significantly increased the tensile strength and mechanical properties of composite gels, while Bnt significantly increased their water absorption capacity. However, to analyze how the performance of a hydrogel changes when Bnt and Kln are added simultaneously and whether two different types of gels can be synergistically applied to produce a good effect, Cheng and coworkers synthesized poly(acrylic acid-*co*-acrylamide)/Bnt/Kln composite hydrogels.[64] The composites showed more swelling in the presence of Bnt than Kln. Increasing Bnt concentration significantly increased the swelling of the gels, while it decreased monotonically with increasing Kln concentration. This decrease observed in the presence of Kln particles can be attributed to the interaction between the carboxylic groups of the polymer chains and the free hydroxyl

groups present on the surface of the clay particles. The formation of new chemical and physical bonds representing new cross-linking points in the hybrid network leads to a decrease in the water absorption ability. A similar result was described by Zaharia and coworkers in the case of polyacrylamide-modified kaolinite containing poly(acrylic acid-*co*-methylene bisacrylamide) nanocomposite hydrogels.[50]

Grn-incorporated hybrid gels have the lowest swelling capacity due to the increased network stiffness because higher crosslinking formation makes it more difficult for water molecules to penetrate the hybrid network. Insufficient space for the water molecules to enter the network results in lower swelling. Therefore, the degree of interaction between the clay surface and the hybrid matrix depends on the hydrogen bonding between the functional groups on the surfaces and the amide group, carbonyl group and hydroxyl group in the hybrid matrix. Penkavova and co-workers investigated the swelling of polyacrylamide hydrogel-based nanocomposites containing graphene, kaolin, or LAPONITE® XLG; the addition of graphene nanosheets or kaolin makes the nanocomposites less stiff, while the addition of LAPONITE® makes them stiffer than the original PAAm hydrogels.

The prepared kaolin and LAPONITE® nanocomposites swell less in water than the original hydrogels, while the graphene nanocomposites show no obvious tendency.[65] Ibraeva and coworkers reported similar swelling tendency for the swelling capacity of PAAm-based organic–inorganic hybrid composite materials prepared using bentonite, montmorillonite, kaolin as well as silica and titanium dioxides in the following order: PAAm/bentonite > PAAm/TiO_2 > PAAm/SiO_2 > PAAm/kaolin ≈ PAAm/montmorillonite.[40] Wu and coworkers prepared starch-*graft*-AAm/clay composites containing kaolinite, sercite and bentonite by graft-copolymerization reaction among AAm and potato starch.[66] Due to moderate dispersion of kaolinite in the water and cross-linking extent with AAm and starch, the composites doped with kaolinite had higher water absorbency when compared with those doped with sercite and bentonite. Since the hydration and distension of bentonite is larger than those of sercite and kaolinite, bentonite tend to dissolve more easily and produce much more particulates in water. Therefore, the crosslinking density of the composites containing bentonite was larger than that of containing sercite and kaolinite.[66] For the swelling of pineapple peel carboxymethyl cellulose-*g*-poly(acrylic acid-*co*-acrylamide)/graphene oxide hydrogels, increasing the graphene oxide content leads to a decrease in the swelling ratio, since the incorporation of graphene oxide increases the cross-linking density of hydrogels. It may lead to the dominance of graphene oxide/polymer interactions over polymers/water interactions, which probably hinders the swelling process of the hydrogels.[10]

Multi-stimuli responsive-swelling depending on the filler-type

Fig. 6 and Fig. S4 (ESI†) presents the equilibrium volume swelling ratio of hybrid gels as a function of swelling pH. Since

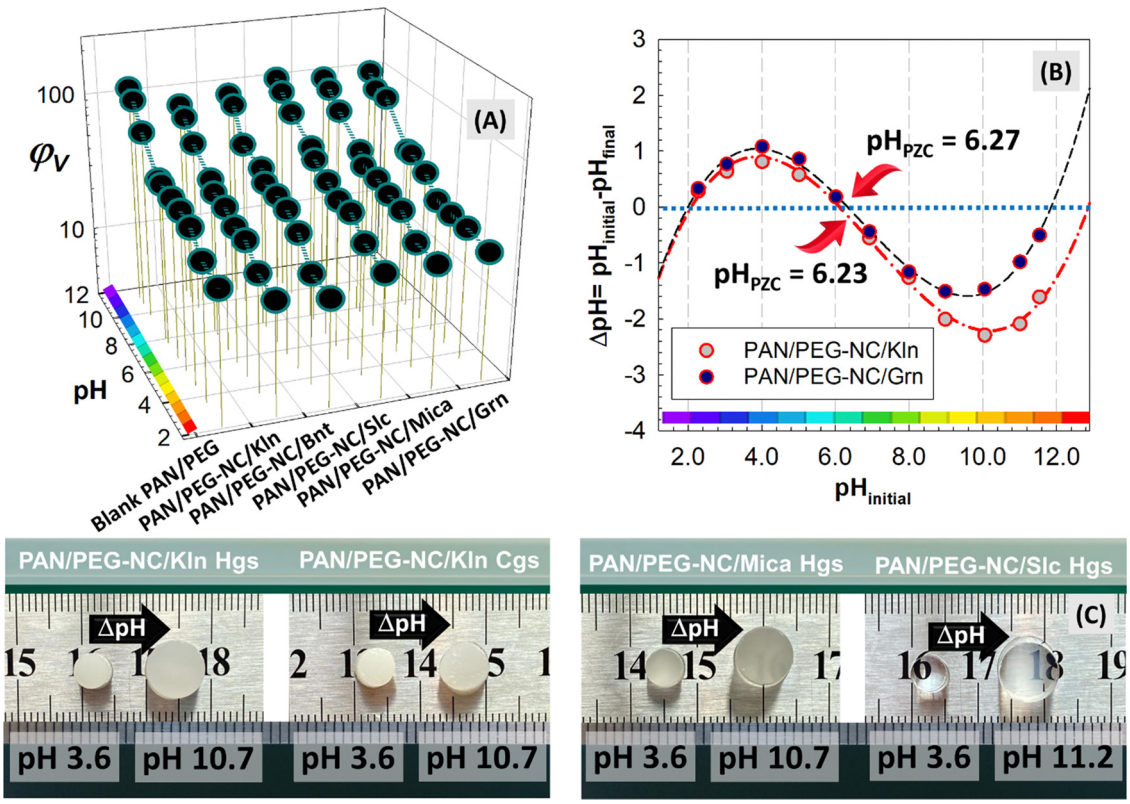

Fig. 6 The equilibrium volume swelling ratio of hybrid hydrogels as a function of swelling pH (A), pH_{PZC} point of hybrid PAN/PEG-NC gels doped with Kln and Grn (B). Optical images of hybrid gel containing Kln, Mica and Slc after swelling in pH solutions (C).

the swelling properties of anionic hydrogels are closely affected by their charge density, the swelling of hybrid gels prepared by adding different fillers to modulate the charge density in the copolymeric network containing anionic sodium acrylate at a fixed 6% mol ratio were investigated. An alternative approach to modulate the charge density of anionic hybrid structure is based on manipulating the degree of ionization of carboxylic acids in the polymer chains by adjusting pH of the surrounding swelling medium. The swelling tendency of hybrid gels is directly affected by the changes in charge density. The swelling profile of PAN/PEG gels containing different fillers is significantly lower under strong acidic conditions, increasing up to pH 6.0, and the hybrids continue to swell, although this increase is slower in the range of pH 6.0–8.0, after pH 8.0, the swelling rate of hybrids increases rapidly with increasing pH levels. The pH of all samples was measured before the experiment and after 48 h of swelling equilibrium, and the same amount of gel was used to measure how the samples were affected by the pH change. According to the plot in Fig. 6(B), the point in which the ΔpH value intersects the *x*-axis is defined as the point of zero charge (pH_{PZC}) and the pH_{PZC} of Grn-doped hybrid PAN/PEG-NC/Grn gels was found to be 6.27 and that of Kln nanoclay-doped PAN/PEG-NC/Kln gels was 6.23, which implies that at $pH < pH_{PZC}$, the hybrid gel surface is positively charged due to the protonation whereas it acquires negative charge above pH_{PZC}. These results provide significant insights into the electrostatic repulsion and attraction interactions affecting the dye adsorption capacity of the adsorbent. Below pH 6.2, the repulsion between the positive surface of hybrid gels and cationic dye molecules impedes the uptake. With an increase in pH, the electrostatic attraction between negatively charged surface and cationic dye molecules enhances the removal efficiency. At $pH < 6.0$, the internal H-bonding within hybrid network converts most of the carboxylate anions in the polymer chains into carboxy acid groups. This transformation eliminates the negative ion repulsion in the hybrid structure, strengthens the H-bonding relationship between the carboxy and amide groups, and thus increases the degree of physical cross-linking. In this pH range, the hybrid structure does not tend to swell, and the gels experience a shrinkage state as seen in Fig. 6(A). As pH value increases in the range of 5.4–8.0, the negatively charged groups within the hybrid network increase due to the ionization of the carboxyl groups, and the increased negative charge density induces the electrostatic repulsion, causing the molecular chains in the hybrid to stretch significantly. Thus, the hybrid gels tend to absorb a large amount of water and swell intensively as presented in the images in Fig. 6(C).

Among the clays incorporated, Slc-integrated hybrid PAN/PEG-NC/Slc gels exhibited high swelling degree in basic pH region since the surfaces of SiO_2 particles have a large number of hydroxyl groups and therefore tend to form H-bonding through van der Waals forces. The ionization of pendant acidic groups in basic pH region enhanced the relaxation of polymer segments because of the elimination of H-bonding. Since most of the carboxylate groups in copolymer PAN chains were protonated under acidic pHs, the acidic functional groups in the network exist as –COOH groups and thus, the main anion–anion repulsive forces between the negatively charged carboxylate groups attached to the network chains were mainly eliminated. As a result, the swelling ratio of hybrid gels were considerably lower since the pores inside the network were not expanded effectively. The existence of H-bonding interactions between –COOH groups in the network creates additional crosslinking sites, and this restricts the movements of polymer segments and results in the relatively lower swelling ratio. Moreover, in the copolymer PAN matrix, the linear PEG chains are held by H-bonding between protons of the amide groups and oxygen atoms of PEG. Replacing sodium with protons in acidic pH values results in additional H-bonding between the oxygen of PEG and the protons of carboxylic acid groups. The trend was in accordance with the swelling-pH dependencies of hydrogels carrying weak acid functional groups.[67] Devine and coworkers prepared pH-responsive poly(acrylic acid-*co*-*N*-vinyl pyrrolidone) gels forming hydrogen bonding between the –COOH of polyacrylic acid and –C═O of the poly(*N*-vinyl pyrrolidone). The swelling of hydrogels at basic pH region is significantly different from that in acidic pH region which makes the resulting hydrogels suitable for gastric drug delivery systems.[68]

Fig. 7 compares the equilibrium volume swelling ratio of hybrid hydrogels as a function of the ionic strength of salt solution of NaCl and $CaCl_2$, respectively. The results for hybrid cryogels were collected in Fig. S5 (ESI†). The swelling capacity of hybrids was significantly affected by the salt solutions, the amount of absorption decreased due to the decrease in osmotic pressure between the gel and aqueous phases in salt solutions. The swelling showed a tendency to decrease depending on both the ''type'' and ''ionic strength'' of the salt added to the swelling medium. With increasing the ionic strength, the swelling decreases due to the decrease in the osmotic pressure difference between the hybrid network and the external salt solution. In addition, the penetration of counter ions Na^+ and Ca^{2+} into the network and a more pronounced screening effect of these ions on anionic groups $–COO^-$ also become important. As the charge of cation increased, the degree of cross-linking increased and hybrid gels showed less swelling in $CaCl_2$ solutions regardless of the filler-type. The swelling behavior of polyvinyl alcohol/carboxymethyl cellulose hydrogels doped with graphene oxide and bentonite in 0.9% NaCl solution is consistent with this study, with bentonite-doped gels showing greater swelling than graphene oxide-doped gels.[10] Pourjavadi and coworkers studied the swelling of composites based on kappa-carrageenan prepared by graft copolymerization of acrylamide in the presence of bentonite. The composites-doped with bentonite showed less swelling capacity in $CalCl_2$ solutions compared to NaCl.[69] Fig. S6 (ESI†) presents the equilibrium volume swelling ratio of hybrid hydrogels as a function of swelling temperature and the optical images of temperature-swelling hybrid gels containing Kln, Mica, and Slc were presented for visual comparison. The swelling ratio of hybrid gels increased significantly with an increase in the temperature between 25 °C and 35 °C. Although the increase in the swelling

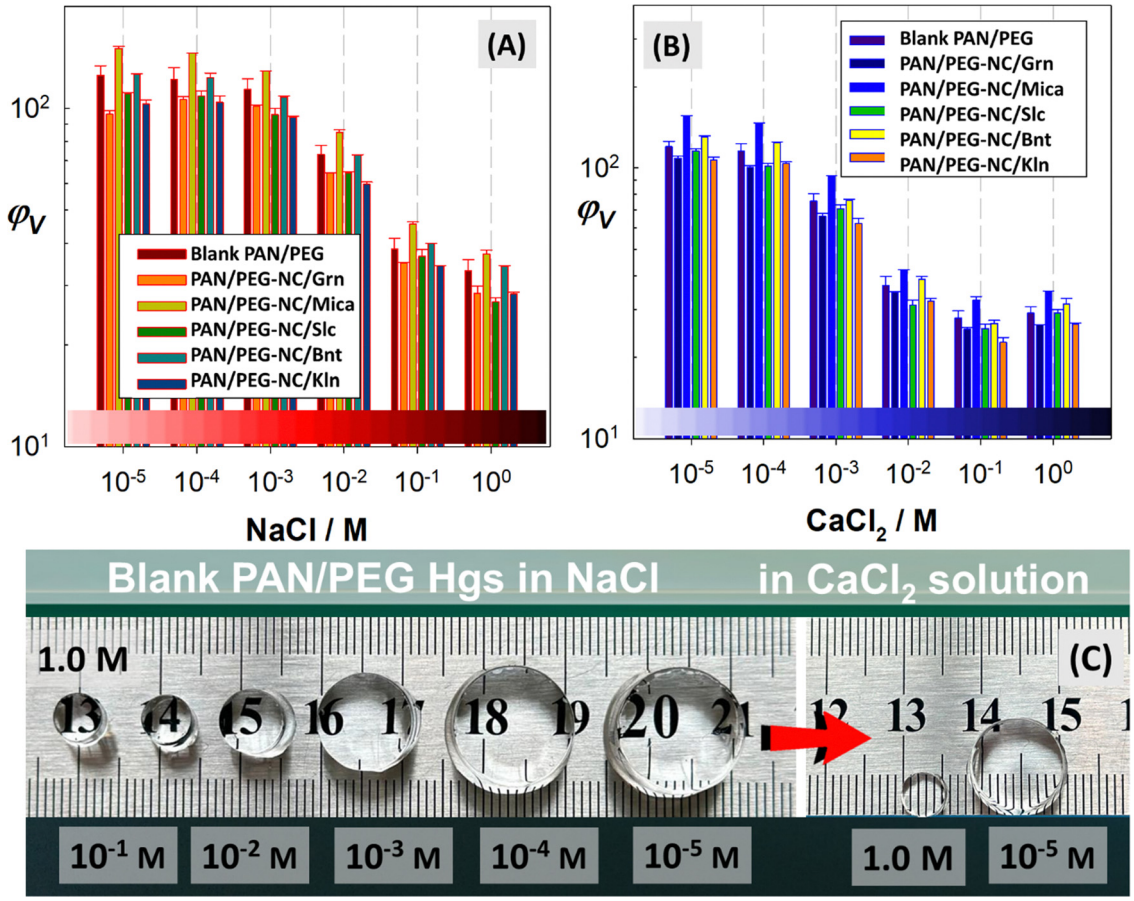

Fig. 7 The equilibrium volume swelling ratio of hybrid hydrogels as a function of the ionic strength of salt solution of NaCl (A) and $CaCl_2$ (B), respectively. Optical images of blank PAN/PEG gels in salt solutions of different ionic strengths (C).

ratio slowed down with further increase in the temperature, the hybrid gels maintained their swollen-state compared to the ambient temperature. The results for hybrid cryogels were presented in Fig. S4 (ESI†). At low swelling temperatures, the interaction of the hybrid chain networks with water molecules causes the swelling by expanding the chains, which occurs through the entanglement of interpenetrating polymer network. However, increasing the temperature disrupts the hydrogen bonds between the interpenetrated chains and increases the swelling ratio. Similar results were reported by Li and coworkers for the temperature-dependent swelling of polyacrylamide/LAPONITE® hydrogels.[70] The swelling experiments were performed at 25, 35, and 60 °C and it was found that the increase in temperature significantly increased the swelling of nanocomposites.

Effect of filler incorporation on dynamic swelling of hybrid gels

Fig. S7 (ESI†) shows the dynamic swelling of filler-integrated hybrid hydrogels in pH 11.2 and deswelling in pH 2.1. The swelling of hybrid gels-doped with various fillers varied depending on the relative contribution of water diffusion and relaxation of cross-linked polymer chains. While the swelling of hybrid hydrogels is slower and the time it takes to reach equilibrium is longer, the swelling rate of cryogels is higher due to their porous structure and it is shorter to reach the plateau region. The absorbency of the filler-integrated hybrid gels increased from pH 2.1 to 11.2, and reversibility to pH 2.1 was achieved, and a gradual, reproducible swelling change of hybrid gels was demonstrated with changing pH.

At pH 11.2, hybrid cryogels showed different swelling tendency according to the filler type due to anion–anion repulsive electrostatic forces, while at pH 2.1, they shrank within a few minutes due to the protonation of carboxylate groups. This sharp swelling–deswelling behavior of cryogels in particular makes them suitable candidates for controlled drug delivery systems. To explain the swelling mechanism of hybrid gels, Peppas power law equation model presented in eqn (S1) (ESI†) (Table S5, ESI†) was used to analyze the experimental data and the curves were presented in Fig. S7(C) (ESI†). Using this model, the dynamic swelling constants k which is the swelling rate constant, and the characteristic exponent n describing the mode of the water transport mechanism were determined (Table S6, ESI†). As the values of diffusional exponent determined from this model for Bnt, Kln, Slc, Mica and Grn-integrated PAN/PEG-NC gels ranged between 0.1153–0.1508, the diffusion of water is Fickian diffusion and the process is diffusion-controlled with a much lower the diffusion rate than the relaxation of hybrid matrix. The diffusion of water into the

filler-doped hybrid structures can be quite complicated due to polar or non-polar interactions, dynamic inhomogeneity in the amorphous phase, and polymer dynamics resulting from solvation. Initially, the water molecules interact strongly with the functional groups such as amide groups in the hybrid PAN/PEG-NC structure, plasticizing the soft amorphous phase and leading to increased mobility of the chains. In the hybrid structure, the presence of nanofillers such as Bnt, Kln, Slc, Mica and Grn creates a mobility gradient in the amorphous phase, and due to these hard fractions, not all amorphous phases may be equally accessible to water molecules. Preda and coworkers studied the diffusion of water in polyamides to determine the influence of polymer relaxations and the differences in the mobility of amorphous phase by NMR.[71] It has been suggested that diffusion is limited by the change in conformation of amide groups in polyamides, depending on the relaxation time of hydrogen bonds between water molecules and amide groups, while a diffusion mechanism based on the retention of water molecules between neighboring amide groups has been proposed. Zhang and coworkers prepared semi-IPN hydrogels based on poly(acrylamide-*co*-acrylic acid) and linear polyallyamine and using oscillatory swelling techniques, pH on–off switching properties of the hydrogels were tested for theophylline as a model drug. semi-IPN hydrogels released the loaded drug completely within 150 min with a non-Fickian mechanism where both diffusion and polymer relaxation control the overall rate of water uptake.[72]

In addition, the Schott second-order dynamic model presented in eqn (S2) (ESI†) was used to analyze the experimental data. The plots of average swelling rate $t/\varphi(t)$ *versus* swelling time t with straight lines indicated that the swelling process of hybrid gels in pH 11.2 solutions follows second-order swelling kinetic model. Based on this model, the initial swelling rate of hybrids was used to determine the values of k_s, the constant rate for swelling, by fitting experimental data shown in Fig. S7(D) (ESI†). The rate of relaxation of chain segments in the hybrid network is related to the initial swelling ratio of gels. At pH 11.2, the ionization tendency of carboxylate groups increases further, leading to a stronger electrostatic repulsion, which favors the relaxation of the polymer network. Rapid relaxation allows the water molecules to penetrate the network more easily, thus increasing the initial swelling ratio. However, it has also been reported that at high pH values, the mobility of the polymer network decreases due to the screening effect of sodium cations, which limit the diffusion of water molecules into the polymer network. Mohan and coworkers prepared a series of semi-IPNs composed of poly(acrylamide-*co*-sodium acrylate) with different amounts of a blood-compatible polymer poly(vinylsulfonic acid sodium salt). Due to the incorporation of carboxylic and sulfonic repeating units into the networks, a stepwise swelling and deswelling behavior was detected on altering the physiological solution; glucose and synthetic urine.[73]

Adsorption ability of filler-integrated hybrid PAN/PEG NC-gels

Although numerous experimental studies have been presented on the adsorption of organic dyes onto nanocomposites, usually limited to a matrix-additive and dye combination, comparative studies on the adsorption ability of gels containing different inorganic components are very limited. For this purpose, anionic PAN matrix crowded with PEG chains was combined with five different additives and compared as adsorbents for cationic methylene blue (MB) dye. It can be clearly observed from Fig. 8 that the initial rate of MB removal increased sharply with time and reached maximum within 60 min due to accessibility of active sites and the incorporation of Grn and Slc evidently improved the dye adsorption abilities of the prepared hybrid gels. Taking adsorption of MB as an example of cationic dye, the adsorption capacities of hybrid gels followed NC-Grn (99.2%) > NC-Slc (88.6%) > NC-Kln (76.7%) > NC-Mica (67.7%) > NC-Bnt (57.7%), respectively, showing an obvious enhancement of adsorption ability with Grn-doped gels. The adsorption capacity of Bnt-integrated hybrid gel is quite low for all the tested systems. While hybrid gels containing Grn nanosheets exhibited superadsorbent properties, the adsorption capacity of hybrid gels containing Bnt decreased.

Fig. 8(G) shows the picture of MB solution (10 mg L^{-1}) before and after adsorption for hybrid gels-doped with Slc, Kln, Mica, Bnt and Grn, respectively. The color of solution with Grn-doped PAN/PEG-NC/Grn turned to transparent significantly, especially in comparation with blank PAN/PEG, indicating the beneficial effects of Grn nanosheets on MB adsorption. Penkavova and coworkers studied the MB adsorption of polyacrylamide-based nanocomposites containing graphene, kaolin or LAPONITE® and reported significant increases in adsorption capacity for LAPONITE®, slight increases for graphene and surprising decreases for kaolin nanocomposites.[65] Depending on the hydrogel morphology, medium-sized pores are advantageous for adsorption. MB adsorption by different filler-containing hybrids was investigated as a function of contact time between the phases and the results were analyzed by the adsorption kinetics models; pseudo first-order (PFO),[74] pseudo second-order (PSO),[75] Elovich,[76] intraparticle diffusion model[77] and Avrami kinetic models[78] were tested using the linear and non-linear equations presented in Table S7 (ESI†). The validity of these models was first analyzed by the non-linear analysis in Fig. 9. Linear regression assumes that the experimental data is linear without checking whether the adsorption process or the kinetic trend is linear. The non-linear method would be more suitable for estimating the parameters included in the kinetic rate expression since linear regression assumes that the distribution of points on the line follows a Gaussian distribution and the standard deviation is the same at each point. In the non-linear method, since all the isotherm parameters are kept constant on the same axis, the error distribution does not change as in the linear technique.[79]

Using eqn (S3) (ESI†), PFO kinetic model was tested to determine the rate constant of pseudo-first-order k_1 (min^{-1}) and the adsorption capacity of MB molecules at equilibrium q_e (mg g^{-1}).[74] As the experimental q_e values were not in agreement with calculated q_e values (in Table S8, ESI†) and the values of R^2 were low for most of the adsorption data (Table 2), the

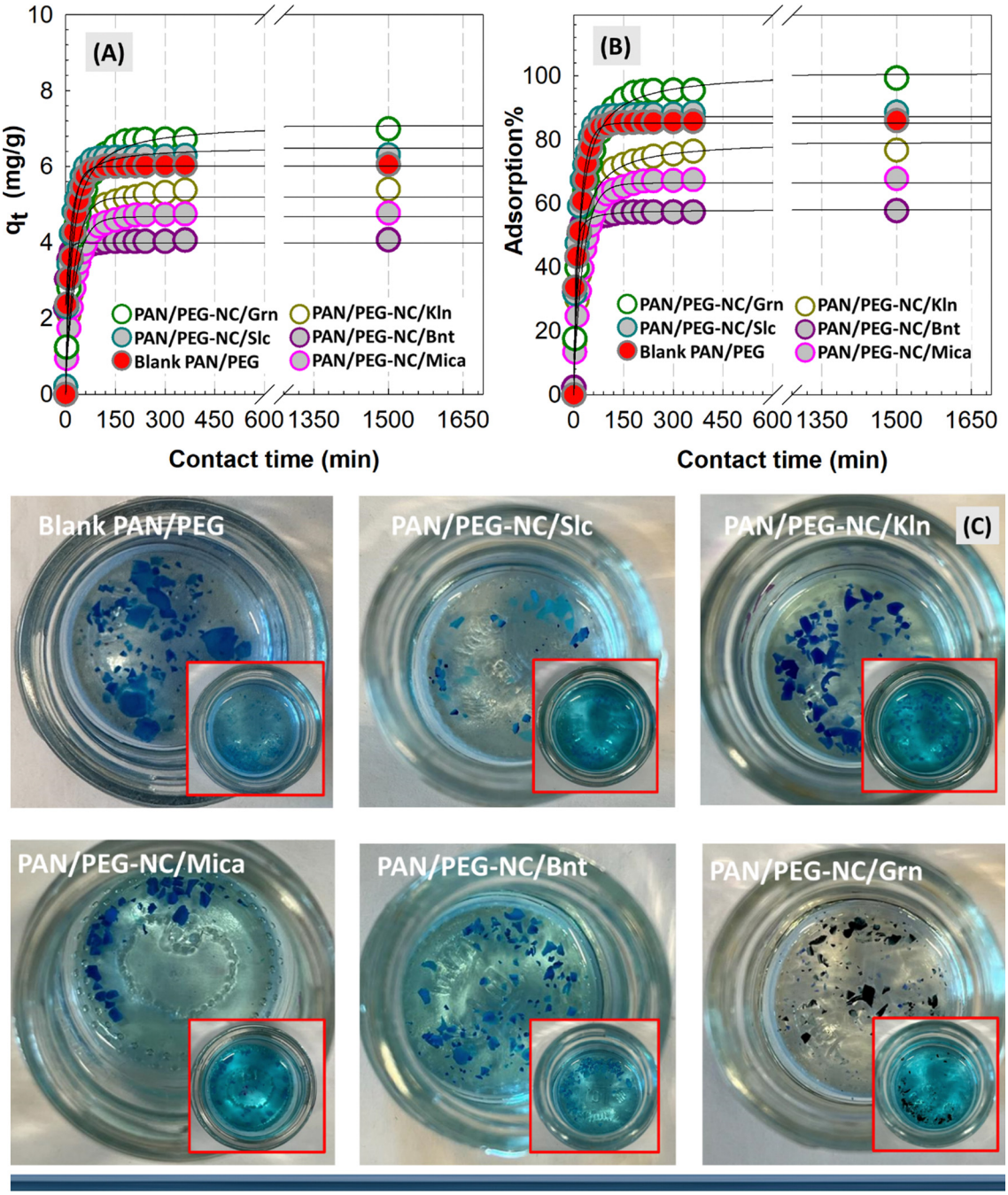

Fig. 8 (A) Adsorption capacity and (B) adsorption% of filler-integrated hybrid gels and (C) optical views of blank PAN/PEG and hybrid PAN/PEG-NC gels during adsorption. (The fixed experimental conditions: MB concentration: 10 mg L^{-1}, adsorbent mass: 10 mg, t = 6 h, V_{dye} = 20 mL, stirring rate = 180 rpm and T = 23 °C.)

adsorption process of MB onto hybrid gels does not follow the PFO model. As the non-linear fit of PSO model showed high R^2 values and closely related calculated q_e values, the linear form of this model was tested for the whole hybrid systems as follows:[75]

$$\frac{dq_t}{dt} = k_2(q_e - q_t)^2, \quad \frac{t}{q_t} = \frac{t}{q_e} + \frac{1}{k_2 q_e^2} \tag{7}$$

where k_2 is the rate constant of PSO model (g mg^{-1} min^{-1}). In Fig. S8(A) (ESI†), the plot t/q_t against time t for each hybrid gel system is presented, and the linear relationships required for the applicability of the PSO kinetic model were obtained. From the slope and intercept of the curves, the values of k_2 and experimental q_e for each hybrid-system were determined. As seen, the model showed good agreement between the experimental and calculated q_e values (Table S8, ESI†) and the R^2 values from linear (Table S9, ESI†) and non-linear fitting (Table 2) were higher than 0.99 and closer to unity for all hybrid

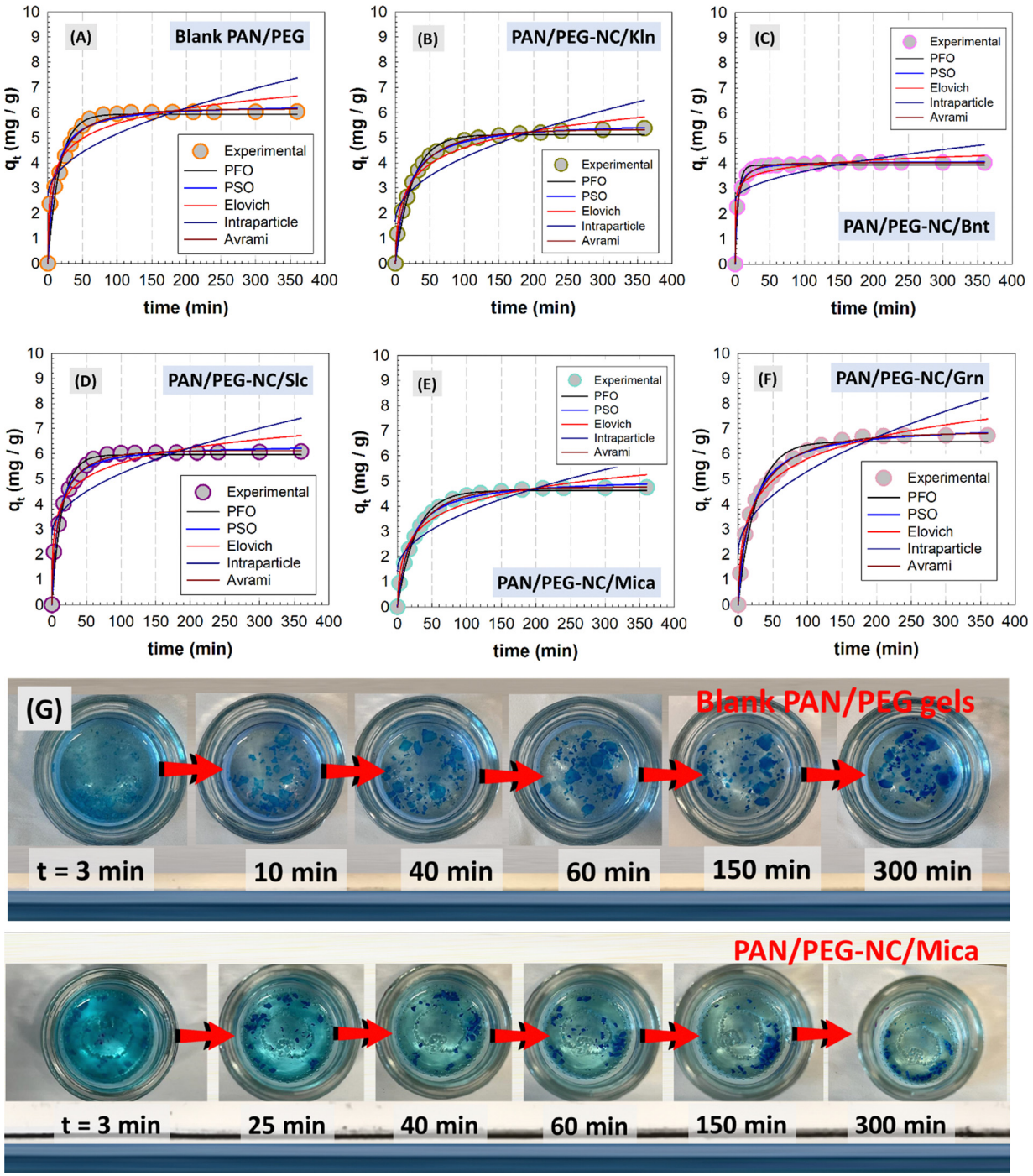

Fig. 9 Results of non-linear PFO, PSO, Elovich kinetic model, intraparticle diffusion model and Avrami kinetic model of blank PAN/PEG and (A) and hybrid PAN/PEC-NC gels containing Kln (B), Bnt (C), Slc (D), Mica (E) and Grn (F). Optical views of blank PAN/PEG and mica-doped PAN/PEG-NC/Mica gels during adsorption (G).

system. Based on the comparison of these calculated values, it can be concluded that the PSO reaction rate depends on the amount of MB adsorbed on the hybrid surfaces and the amount adsorbed at equilibrium, as the PSO kinetic equation describe the MB sorption more accurately. Similar result was reported by Gayathri and Palanisamy for MB adsorption onto polyacrylamide/graphite composites and the effect adsorption parameters revealed that PSO and Langmuir model exhibited good correlation with the adsorption kinetic and isotherm data, while H-bonding and electrostatic interactions dominated the adsorption of dye.[80]

To suggest a comprehensive mechanism of MB diffusion into the hybrid gels, the intraparticle diffusion (IPD) model was used based on the fraction of adsorbate molecules expressed in terms of the square root of time by ref. 77:

Table 2 Comparison of non-linearized PFO, PSO, Elovich, Avrami, fractional and intraparticle diffusion kinetic models' rate constants calculated from the experimental data

Pseudo-first order model (PFO)			Elovich model		
Sample	$k_1 \times 10^{-1}$ (min^{-1})	R^2	α (mg g^{-1} min^{-1})	β (g mg^{-1})	R^2
Blank PAN/PEG	0.5907	0.9472	5.6522	1.1676	0.9461
PAN/PEG-NC/Kln	0.4031	0.9804	1.1416	1.0404	0.9713
PAN/PEG-NC/Bnt	2.1294	0.9688	10.029	3.2451	0.9495
PAN/PEG-NC/Slc	0.6723	0.9682	6.6393	1.1830	0.9446
PAN/PEG-NC/Mica	0.3708	0.9874	0.8415	1.1079	0.9651
PAN/PEG-NC/Grn	0.3839	0.9698	1.2939	0.8037	0.9789

Pseudo-second order model (PSO)			Avrami model		
Sample	$k_2 \times 10^{-3}$ (g mg^{-1} min^{-1})	R^2	n_{Av}	k_{AV} (min^{-1})	R^2
Blank PAN/PEG	1.6545	0.9720	6.1453	0.0624	0.9863
PAN/PEG-NC/Kln	1.0321	0.9957	5.3240	0.0378	0.9985
PAN/PEG-NC/Bnt	9.3965	0.9961	4.0215	0.2236	0.9981
PAN/PEG-NC/Slc	1.8420	0.9895	6.1208	0.0696	0.9967
PAN/PEG-NC/Mica	1.0245	0.9953	4.7613	0.0354	0.9991
PAN/PEG-NC/Grn	0.7784	0.9957	0.6499	6.8416	0.9984

$$q_t = k_{eff} t^{1/2} + C \quad (8)$$

where k_{diff} is the rate constant of IPD model (mg g^{-1} min$^{1/2}$) and C is the thickness of adsorbent determined from the slope and intercept of linear plot of q_t *vs.* $t^{1/2}$ in Fig. S8(B) (ESI†). All linear regions have different slopes away from the origin for different filler-doped hybrids, indicating that MB adsorption is regulated by a multi-step mechanism. The slope is larger in the first stage (Table S9, ESI†), where the MB dye is transferred to the outer surface of the hybrid gel by diffusion into the boundary layer. In the second stage, MB molecules continuously diffuse to the adsorbent sites of the pores in hybrid matrix by intraparticle diffusion. Based on Elovich model[76] using eqn (S5) (ESI†), the parameters $\propto$ (mg g^{-1} min^{-1}) which is the initial rate of MB adsorption, and β (g mg^{-1}) which defines the extent of surface coverage were determined (Table 2). The correlation coefficients of Elovich kinetic model were more than 0.9446, revealing the good model applicability. In addition, for Bnt-doped hybrid gels, the higher initial rate coefficient α of MB adsorption and the β coefficient based on surface coverage are proportional to the low adsorption capacity.

Using eqn (S6) (ESI†), Avrami kinetic model[78] was applied to determine the coefficients k_{Av} and n_{Av} which are Avrami kinetic constant and the model exponent time related to the adsorption mechanism, respectively. Since good fit to the Avrami model was obtained with high R^2 values (>0.99), the adsorption mechanism may follow multiple kinetic orders that change during the contact of adsorbate with adsorbent. For the adsorption of MB onto filler-doped hybrid gels, the values of standard Gibbs free energy change ΔG° were calculated by van't Hoff equation as; $\Delta G^\circ = -RT \ln K_c$, where K_c is the equilibrium stability constant of adsorption which was determined as $K_c = q_e/C_e$. According to the results of thermodynamic calculations shown in Table S8 (ESI†), negative ΔG° values indicate that the adsorption process is spontaneous for all hybrid gels. The decreasing order in ΔG° values (NC-Grn > NC-Slc > NC-Kln > NC-Mica > NC-Bnt) indicated greater driving force and thus faster adsorption capacity.

Adsorption isotherms of filler-integrated hybrid PAN/PEG NC-gels

To illustrate the relation between the amount of adsorbed MB (mg g^{-1}) per unit mass of adsorbent at equilibrium and the residual MB concentration (mg L^{-1}) in solution, the adsorption isotherm studies were performed by varying the initial MB concentration between 20–100 mg L^{-1}. While the adsorption kinetics of hybrid gels loaded different fillers and their selectivity to MB dye were investigated at steady state, Slc- and Grn-loaded hybrid structures with efficient adsorption were selected in the adsorption isotherm studies. Fig. 10 shows the adsorption capacity of MB onto Slc and Grn-doped hybrid gels, utilizing 10 mg L^{-1} adsorbent dosage, 24 h contact shaking time, pH 7 at 23 °C. The obtained results from the adsorption isotherm models were analyzed by five kinetic models including Langmuir, Freundlich, Redlich–Peterson (R–P), Sips, and Dubinin–Radushkevich (D–R) isotherm models[74] given by eqn (S8)–(S12) in Table S10 (ESI†). The adsorption capacity tends to increase significantly with the increase of the initial MB concentration as seen in Fig. 10(A). As MB concentration increased from 20 to 100 mg L^{-1}, the adsorption capacity of blank PAN/PEG gel, Slc and Grn-integrated hybrid gels increased between 9.93–81.74 mg g^{-1}, 14.0–84.8 mg g^{-1} and 19.6–95.1 mg g^{-1}, respectively. Increasing MB concentration provides an enhanced driving force to overcome the mass transfer resistance of the dye molecules from the aqueous phase to the solid phase.

Fig. 11 shows the plots of non-linear Langmuir, Freundlich, Redlich–Peterson, Sips, and D–R isotherms for adsorption of MB onto hybrid PAN/PEC-NC gels containing Slc and Grn. In Fig. 11(A) and (B), the blank PAN/PEG and Slc-doped hybrid gels fit the S-type isotherm, the slope initially increases with the

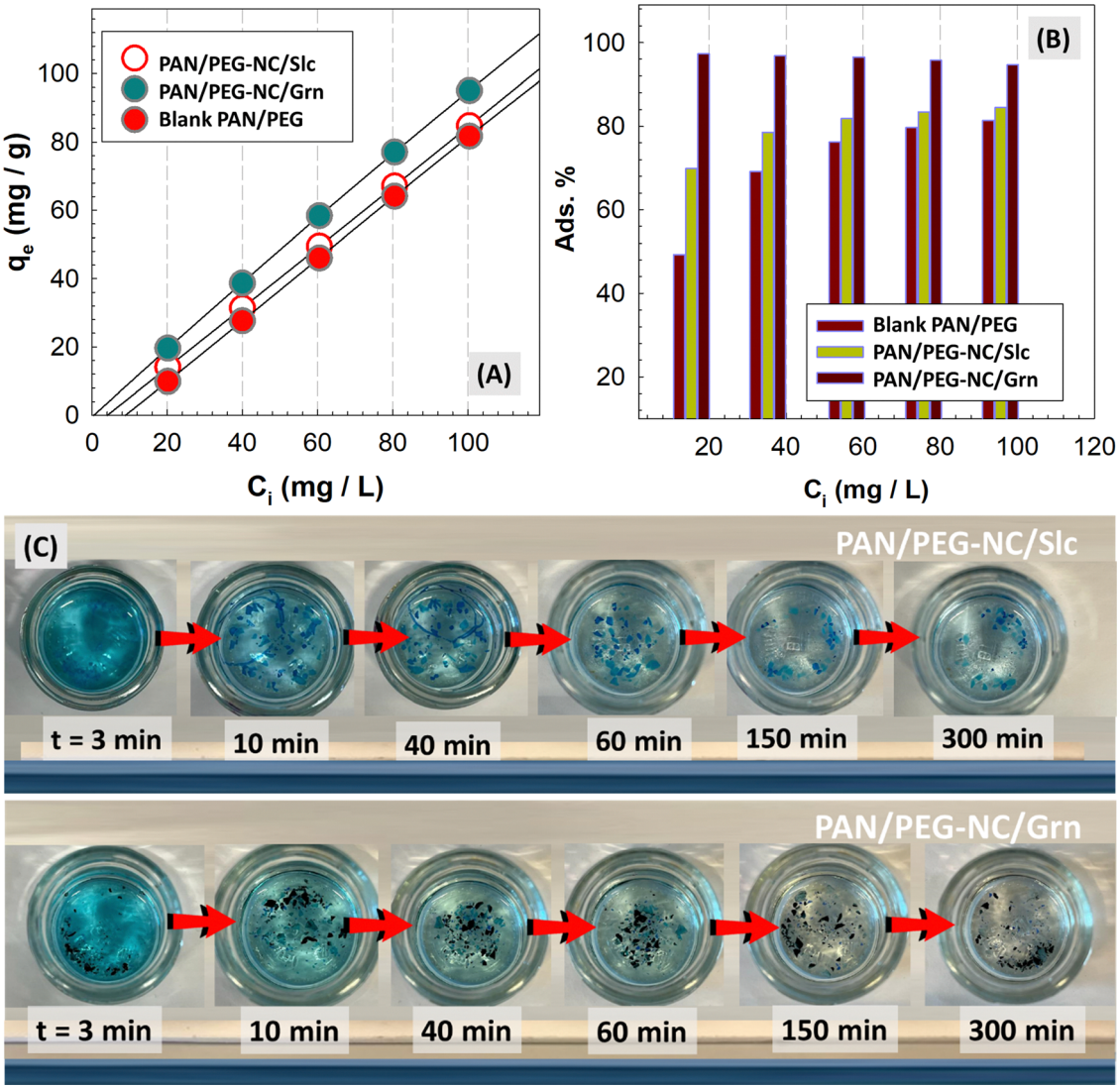

Fig. 10 Adsorption capacity q_e (A) and adsorption% (B) of hybrid PAN/PEC-NC gels and optical views of Slc and Grn-integrated hybrid gels during adsorption (C). (The fixed experimental conditions: MB concentration: 20–100 mg L^{-1}, adsorbent mass: 10 mg, V_{dye} = 20 mL, time = 24 h, stirring rate = 180 rpm and T = 23 °C.)

adsorptive concentration and then decreases. This trend indicates that the hybrid surface has a low affinity for the dye at low concentrations and increases at high concentrations. The L-shaped isotherm of Grn-doped PAN/PEG-NC/Grn gel given in Fig. 11(C) shows a decreasing slope with increasing concentration as the vacant adsorption sites decrease as the hybrid surface is covered. Therefore, the high affinity of Grn-doped hybrid gels for MB at low concentrations then decreases with increasing dye concentration. The correlation coefficients and isotherm parameters were presented in Table 3. Based on the non-linear Langmuir isotherm model using eqn (S8) (ESI†), higher R^2 value was obtained for Grn-doped hybrid gel, while the R^2 values were lower for the blank and Slc-doped gels. The monolayer capacities of Slc and Grn-doped adsorbents are compatible with the experimental values; 83.56 and 96.49 mg g^{-1}, respectively, which may indicate the presence of functional groups on the surfaces as well as the higher surface areas of the hybrid structures. Using eqn (S9) (ESI†), Freundlich adsorption model describing the multilayer adsorption with heterogeneous surface was tested. In this model, where the $1/n_F$ value varying between 0 and 1 represents favorable adsorption conditions, high R^2 values were obtained and the heterogeneity of the surface for Grn nanosheets was supported. The value of n_F reveals that adsorption of MB on PAN/PEG-NC/Grn surface is favorable and confirms high bonding capacity.

The D–R isotherm was tested by eqn (S12) (ESI†) to determine the mean adsorption energy and the characteristics of adsorption. The D–R model suggests that when E values range from 0 to 8 kJ mol^{-1}, the possible adsorption is the physisorption. In Table 3, the values for blank PAN/PEG, Slc and Grn-doped hybrid gels are found to be 1.3350, 4.6220 and 0.7039 kJ mol^{-1}, respectively, suggesting the physisorption process. Sips isotherm model as a combination of the Freundlich and Langmuir isotherm models was used by eqn (S11)

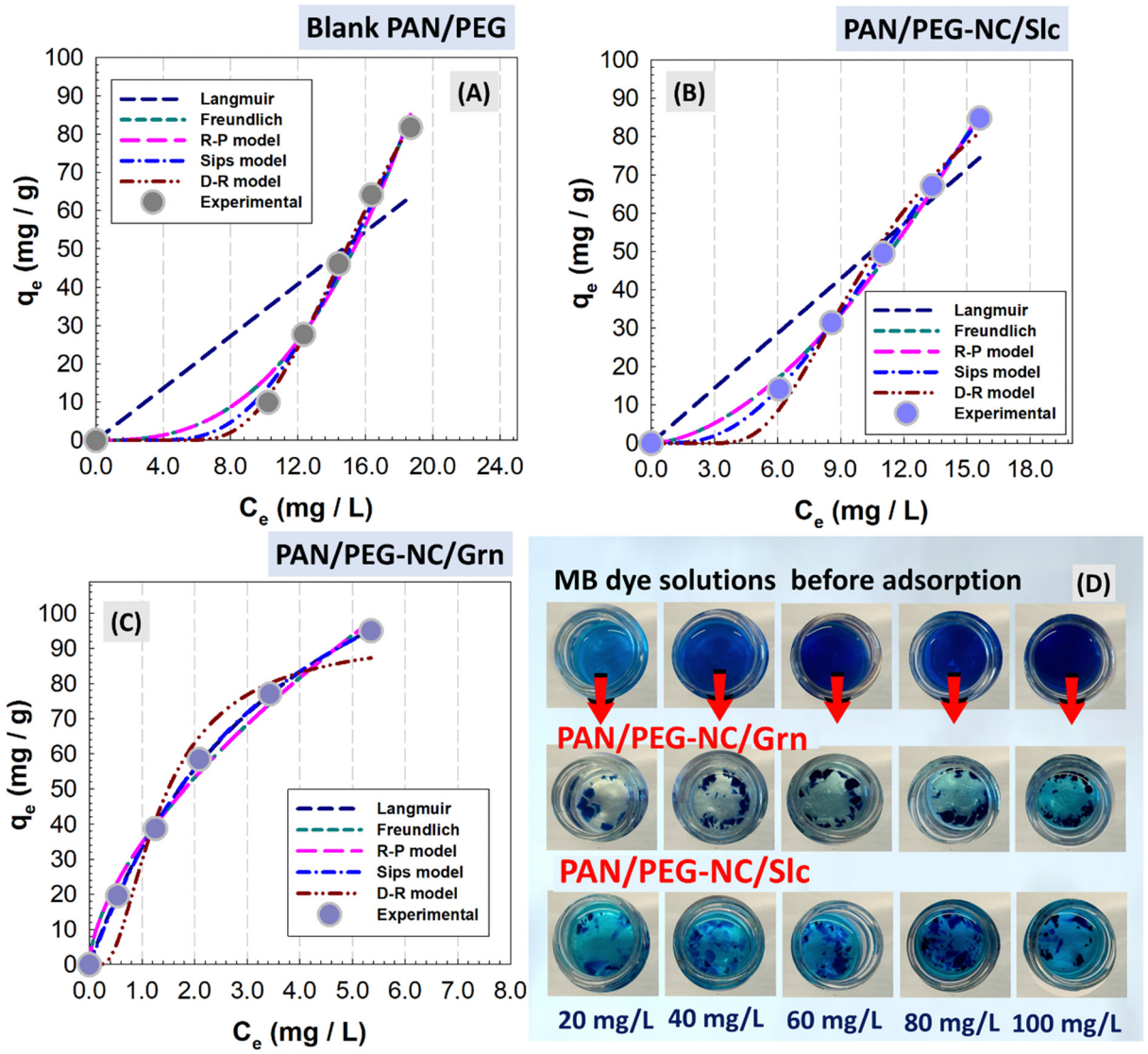

Fig. 11 Results of non-linear Langmuir, Freundlich, Redlich–Peterson, Sips, and D–R isotherms for adsorption of MB onto blank PAN/PEG (A), hybrid PAN/PEC-NC gels containing Slc (B), and Grn (C) and optical images of hybrid cryogels after adsorption of aqueous MB solutions with different concentrations (D).

(ESI†) to analyze the heterogeneous surface in detail. At high adsorbate concentrations, the Sips isotherm approaches the Langmuir isotherm, whereas it approaches the Freundlich isotherm at low concentrations. Using this model, the calculated values of K_S (L g^{-1}) which defined as Sips constant related to energy of adsorption, and the model exponent n_S which can be considered as the parameter characterizing the system heterogeneity were presented in Table 3. The model assumes that when n_S = 1, the Sips equation transforms into the Langmuir equation and indicates a homogeneous adsorption. Since the n_S values in Table 3 are less than 1, the results do not fit the Langmuir model. The relatively low k_S values obtained support the fact that the active sites have different energies during the adsorption process and that the process is multilayered and obeys the Freundlich isotherm. The Sips model best represents the equilibrium data with R^2 values greater than 0.99, indicating heterogeneous surface adsorption of MB on the hybrid. Since the R^2 values of the three models decrease in the order Sips > Freundlich > Langmuir, the results show that the equilibrium data fit the three-parameter model rather than the two-parameter models.

Ahmed and Dhedan showed the successful prediction of MB adsorption on agricultural waste based activated carbons using the Sips isotherm compared to the Langmuir and Freundlich isotherms.[81] The obtained result was attributed to the ability of Sips isotherm to predict wide concentration ranges. Redlich–Peterson (R–P) model given by eqn (S11) (ESI†) including three adjustable parameters was also used as a compromise between Langmuir and Freundlich systems. In this model, the parameters; K_{RP} and β are the R–P constants and the value of β is equal to 1 when this model is reduced to the Langmuir isotherm. According to the results given in Table 3, since only

Table 3 Data from non-linear fitting experimental data on adsorption isotherms of MB dye onto hybrid PAN/PEC-NC gels

Isotherm model	Isotherm parameters	Blank PAN/PEG	PAN/PEG-NC/Slc	PAN/PEG-NC/Grn
Langmuir	q_{max} (mg L^{-1})	76.258	83.567	96.495
	K_L (L mg^{-1})	0.3256	0.4567	0.2545
	R^2	0.7531	0.9146	0.9995
Freundlich	K_F (mg g^{-1}) (mg $L^{-1})^{-1/n}$	0.1327	0.7873	3.4644
	$1/n_F$	2.6867	1.7091	0.6188
	R^2	0.9815	0.9967	0.9927
Redlich–Peterson (R–P)	K_{RP} (L g^{-1}) × 10^{-5}	4.0950	9.3445	9.1356
	α_{RP}	0.328	0.7881	34.647
	β_{RP}	2.6853	1.7087	0.6188
	R^2	0.9815	0.9967	0.9927
Sips	K_S (L g^{-1}) × 10^{-1}	3.9531	0.1710	0.3029
	n_S	0.1620	0.2007	0.9275
	R^2	0.9938	0.9999	0.9996
Dubinin–Radushkevich (D–R)	β (mol^2 J^{-2})	0.2025	0.1261	0.9370
	E (J mol^{-1})	1.3350	4.6220	0.7039
	R^2	0.9992	0.9885	0.9546

the β value for Grn-doped hybrid gels complies with this condition, it is thought that the results obtained with the Sips equation may be more realistic than those obtained with the Langmuir equation.

FTIR spectroscopy was conducted on blank PAN/PEG and hybrid gels with different fillers after adsorption as depicted in Scheme 3. FTIR spectrum of MB presents several bands belonging the axial-deformation vibrations of the C–H bond in polynuclear aromatic rings between 700 and 900 cm^{-1}. The stretching vibration of the aromatic ring at 1582 cm^{-1}, the vibration of the heterocycle skeleton at 1487 cm^{-1}, the symmetric bending vibration of the CH_3 groups in the dimethylamine groups at 1389 cm^{-1} and the CN stretching vibration at 1238 cm^{-1} were the spectral peaks associated with the characterization of MB dye.[82] In the spectral analysis of blank PAN/PEG and hybrid gels, distinct traces of MB were observed, as well as characteristic peaks for the characterization of these gels before adsorption. The bands in the regions 1260–1360 cm^{-1} were attributed to the axial deformation of the C–N bond of aromatic amines,[82] while that of 1030–1240 cm^{-1} were

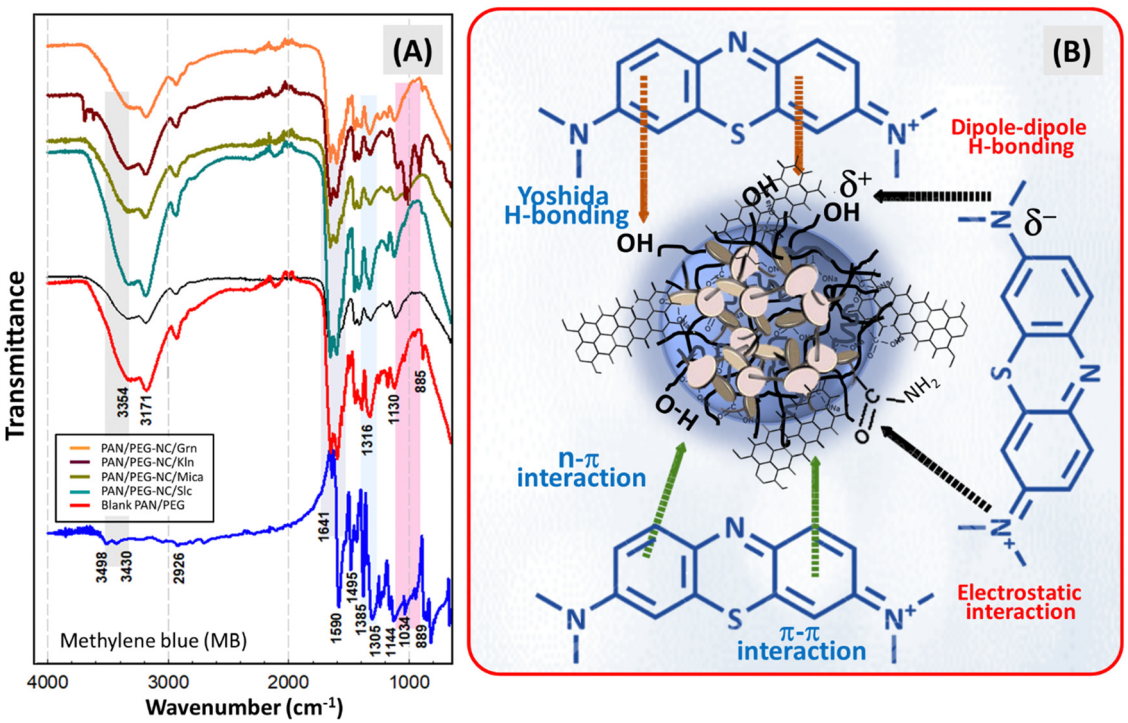

Scheme 3 FTIR spectra of blank PAN/PEG and hybrid gels with different fillers (A) and proposed interactions for cationic MB dye onto anionic hybrid gels (B).

due to the axial deformation vibrations of the C–N bond of aliphatic amines. The intensity of the band between 3300 and 3600 cm^{-1} attributed to both carboxylic acid and phenolic groups changed due to the interaction of these groups with MB dye. Typically, the synergic effect of PAN/PEG matrix and Slc, Bnt, Kln, Mica and Grn nanosheets leads to good adsorption of dye. The results showed that the likely mechanism of cationic MB adsorption by the anionic hybrid PAN/PEG-NC gels involves π–π interaction (π–π electron donor–acceptor interactions) between Grn nanosheets and aromatic ring of MB, n–π interaction (n–π electron donor–acceptor interactions) between oxygen groups of hybrid PAN/PEG-NC network act as electron donors and the aromatic rings of MB act as electron acceptors, dipole–dipole hydrogen bonding between hydroxyl groups (H-donor) of PEG units and the electronegative residue (N lone pair) of MB molecule, and Yoshida hydrogen bonding interaction between –OH groups of PAN/PEG matrix and aromatic rings in MB and the electrostatic interaction between $–NH_2$ group of copolymer PAN chains and the positively charged active sites of cationic MB molecule.

Table S11 (ESI†) lists the comparison of MB adsorption capacity of the prepared hybrid gels with those obtained from different studies reported in the literature. The performance of various polymeric gels used in the removal of MB dye from water was compared with the performance of existing hybrid gels. The distribution of adsorption capacities observed in Table S11 (ESI†) is large from 50 mg g^{-1} to 250 mg g^{-1}. As the adsorption capacity of the gels in Table S11 (ESI†) varies mainly according to the polymer matrix/additive combination, no significant trend can be observed according to the types and contents of the additives. The adsorption capacity is affected by the amount of the substance, whether the adsorbent is dry or wet, the dye concentration, and the presence of salt. It should be noted that direct comparison of the adsorption efficiencies obtained from different systems provides an approximate idea, and the differences between the adsorption capacities in the presented studies will be large due to differences in the experimental conditions. It can be seen that the prepared hybrid gels can be classified as good candidates for the effective adsorbents for cationic dye removal.

Conclusions

A systematic method was used to design anionic poly (acrylamide-*co*-sodium acrylate)/poly(ethylene glycol) hybrid gels at varied reaction parameters. The study provides useful information for the rational design of new generation environmentally friendly, cost effective and efficient hybrid structures for cationic dye removal from wastewater. The partial rearrangements obtained from XRD results confirmed the connection between the nanofiller and PAN/PEG chains. Hybrid gels are tough materials and the integration of nanofillers with different structures was beneficial to enhance the mechanical strength due to the non-covalent or physical crosslinking interaction between the network chains and fillers. The elastic moduli of hybrid PAN/PEG-NC gels incorporated with the same content of inorganic component is in the order NC-Graphene > NC-Silica > NC-Mica > NC-Kaolin > NC-Bentonite. Besides graphene, silica particles played a significant role in the mechanical properties of the hybrid gels. The compressive elasticity corresponds to the improved toughness of hybrid gels based on the energy dissipation mechanism compared to the chemically cross-linked interaction. Among hybrid gels with the same amount of filler, the highest swelling was observed in Bnt-integrated gels, while the least swelling was in Grn-integrated gels. All prepared hybrid gels showed a similar change trend in the swelling ratio with increasing pH values due to the presence of anionic polysodium acrylate units in the structure. Due to the interplay between pH-dependent ionization and electrostatic interactions, hybrid gels have shown the ability to regulate the swelling in response to changes in the surrounding pH between 2.1–11.2. Regardless of the filler-type, the equilibrium water content and the swelling ratio increased significantly with the increase in the temperature of swelling medium. With the increase of ionic strength in salt solutions, especially at very high salt concentrations, the swelling of hybrid gels was strongly suppressed and salting out behavior was observed. By increasing the pH between 2.1 and 11.2, Bnt-doped gel exhibited a swelling ratio 5-fold higher than the initial condition, while the least swelling was observed in the Kln and Mica-doped gels with a 4.1-fold increase. The dynamic swelling kinetics study revealed that the diffusion of hybrid gels was a Fickian mechanism. Under the selected operating conditions and for a contact time of 360 min, the maximum efficiency of MB adsorbed for hybrids containing Graphene and Silica was 99.2% and 88.60%, respectively. Adsorption kinetics and equilibrium adsorption isotherm fitted pseudo-second-order kinetic model and Sips isotherm model well, respectively. The Sips model best represented the adsorption equilibrium data while the adsorption of MB on the hybrid was shown to fit the three-parameter model rather than the two-parameter models. The prepared hybrid gels provided a perspective for new alternative strategies for exploratory small laboratory scale water treatment as a step towards large-scale and long-term applications.

Data availability

All data connected with this work are available upon request to the corresponding author.

Conflicts of interest

There are no conflicts of interest to declare.

Acknowledgements

This work was supported by Scientific Research projects Department of Istanbul Technical University. Project number: 45052.

References

1 F.-M. Cheng, H.-X. Chen and H.-D. Li, *Eur. Polym. J.*, 2020, **124**, 109448.
2 T. Chen, K. Hou, Q. Ren, G. Chen, P. Wei and M. Zhu, *Macromol. Rapid Commun.*, 2018, **39**, 1800337.
3 T. Boyaci and N. Orakdogen, *Appl. Clay Sci.*, 2016, **121–122**, 162–173.
4 A. Amari, F. Mohammed Alzahrani, K. Mohammedsaleh Katubi, N. Salem Alsaiari, M. A. Tahoon and F. Ben Rebah, *Materials*, 2021, **14**(6), 1365.
5 E. P. de Sousa, D. T. de Araujo, V. G. Peixoto, B. F. Ferreira, E. H. de Faria and E. F. Molina., *Appl. Clay Sci.*, 2020, **191**, 105605.
6 P. Aranda, M. Darder, B. Wicklein, G. Rytwo and E. Ruiz-Hitzky, Clay–Organic Interfaces for Design of Functional Hybrid Materials, in *Hybrid Organic-Inorganic Interfaces: Towards Advanced Functional Materials*, ed. M.-H. Delville and A. Taubert, Wiley-VCH Verlag GmbH & Co. KGaA, 2017, pp. 1–84.
7 F. Bergaya, C. Detellier, J.-F. Lambert and G. Lagaly, Introduction to Clay–Polymer Nanocomposites (CPN), in *Developments in Clay Science*, ed. F. Bergaya and G. Lagaly, Elsevier, 2013, ch. 13.0, vol. 5, pp. 655–677.
8 Y. Tang, Q. Wang, B. Zhou, D. Ma, Z. Ma and L. Zhu, *Polym. Polym. Compos.*, 2015, **23**(7), 467–474.
9 H. Hosseini, A. Zirakjou, D. J. McClements, V. Goodarzi and W. H. Chen, *J. Hazard. Mater.*, 2022, **421**, 126752.
10 H. Dai, Y. Huang and H. Huang, *Carbohydr. Polym.*, 2018, **185**, 1–11.
11 N. Limparyoon, N. Seetapan and S. Kiatkamjornwong, *Polym. Degrad. Stab.*, 2011, **96**, 1054–1063.
12 J. Zhang and A. Wang, *React. Funct. Polym.*, 2007, **67**, 737–745.
13 Z. Jiang, X. Cao, Z. Li and L. Guo, *J. Pet. Explor. Prod. Technol.*, 2016, **6**, 93–99.
14 X. Tan, F. Liu, L. Hu, A. H. Reed, Y. Furukawa and G. Zhang, *Appl. Clay Sci.*, 2017, **135**, 313–324.
15 A. B. Mapossa, A. H. da Silva Júnior, C. R. S. de Oliveira and W. Mhike, *Polymers*, 2023, **15**, 3443.
16 L. H. Gaabour, *Results Phys.*, 2017, **7**, 2153–2158.
17 L. T. Chiem, L. Huynh, J. Ralston and D. A. Beattie, *J. Colloid Interface Sci.*, 2006, **297**, 54–61.
18 Y. C. Lee, C. W. Liew, M. H. Buraidah and H. J. Woo, *Opt. Mater.*, 2023, **140**, 113791.
19 C. Xiong, F. Wei, W. Li, P. Liu, Y. Wu, M. Dai and J. Chen, *ACS Omega*, 2018, **3**(9), 10716–10724.
20 I. M. Ashraf and A. A. El-Zahhar, *Results Phys.*, 2018, **11**, 842–846.
21 S. Zhang, F. Hu, J. Li, L. Lv and H. Lu, *Adv. Mater. Sci. Eng.*, 2021, **12**, 2588784.
22 E. Balan, A. M. Saitta, F. Mauri and G. Calas, *Am. Mineral.*, 2001, **86**, 1321–1330.
23 B. Zhang, Y. Li, X. Pan, X. Jia and X. Wang, *J. Phys. Chem. Solids*, 2007, **68**, 135–142.
24 B. Tanc and N. Orakdogen, *J. Polym. Sci., Part B: Polym. Phys.*, 2019, **57**(24), 1758–1778.
25 R. Liang and M. Liu, *J. Appl. Polym. Sci.*, 2007, **106**, 3007–3017.
26 C. Ji, X. Wei, H. Wang, L. Chao, J. Li and X. Qi, *J. Dispersion Sci. Technol.*, 2019, **42**(4), 569–580.
27 B. Tanc and N. Orakdogen, *Soft Matter*, 2019, **15**(15), 3208–3226.
28 A. Tabak, N. Yilmaz, E. Eren, B. Caglar, B. Afsin and A. Sarihan, *Chem. Eng. J.*, 2011, **174**, 281–288.
29 J. Thomasukutty, C. G. Soney, M. G. Maya, J. M. Hanna, W. Runcy and T. Sabu, *Ind. Eng. Chem. Res.*, 2014, **53**(43), 16820–16831.
30 S. D. Chaudhuri, A. Mandal, A. Dey and D. Chakrabarty, *Appl. Clay Sci.*, 2020, **185**, 105405.
31 A. Saad, I. Bakas, J.-Y. Piquemal, S. Nowak, M. Abderrabba and M. M. Chehimi, *Appl. Surf. Sci.*, 2016, **367**, 181–189.
32 B. Kalkan and N. Orakdogen, *Soft Matter*, 2022, **18**(24), 4582–4603.
33 H. Ramadan, T. Coradin, S. Masse and H. El-Rassy, *Silicon*, 2011, **3**, 63–75.
34 R. Al-Oweini and H. El-Rassy, *J. Mol. Struct.*, 2009, **919**, 140–145.
35 H. Wang, L. Chao, X. Wei, J. Li, C. Ji, B. Wang, X. Qi, P. Hu, Y. Ying and M. Tian, *Colloids Surf., A*, 2019, **583**, 123982.
36 L. Zhu, C. Feng, B. Peng, X. Hui, X. Bai and Z. Yu, *Molecules*, 2023, **28**, 7106.
37 N. S. O. Besli and N. Orakdogen, *Soft Matter*, 2021, **17**, 9371–9386.
38 A. Beran, *Rev. Mineral. Geochem.*, 2002, **46**(1), 351–369.
39 M. Singha and L. Singh, *Indian J. Pure Appl. Phys.*, 2016, **54**, 116–122.
40 Z. E. Ibraeva, A. A. Zhumaly, E. Blagih and S. E. Kudaibergenov, *Macromol. Symp.*, 2015, **351**, 97–111.
41 Z. Vajglova, N. Kumar, M. Peurla, J. Peltonen, I. Heinmaa and D. Y. Murzin, *Catal. Sci. Technol.*, 2018, **8**(23), 6150–6162.
42 G. W. Brindley and J. Lemaitre, Thermal oxidation and reduction reactions of clay minerals: in chemistry of clays and clay minerals, in *Longman Scientific and Technical (Essex)*, ed. A. C. D. Newman, Mineralogical Society, London, 1987, pp. 319–370.
43 T. Wan, Z. Zhou, R. Huang, C. Zou, M. Xu, W. Cheng and R. Li, *Appl. Clay Sci.*, 2014, **101**, 199–204.
44 D. H. S. Souza, C. T. Andrade and M. L. Dias, *Polímeros*, 2014, **24**, 20–24.
45 C. Akinyi and J. O. Iroh, *Polymers*, 2023, **15**, 299.
46 B. Yu, X. Wang, W. Xing, H. Yang, X. Wang, L. Song, Y. Hu and S. Lo, *Chem. Eng. J.*, 2013, **228**, 318–326.
47 M. C. Ruiz-Cañas, H. I. Quintero, L. M. Corredor, E. Manrique and A. R. Romero Bohórquez, *Polymers*, 2020, **12**(5), 1152.
48 J. Jang and H. Park, *J. Appl. Polym. Sci.*, 2002, **83**, 1817–1823.
49 H. U. Jamo and S. G. Abdu, *Sci. World J.*, 2014, **9**(3), 29–30.
50 A. Zaharia, A. Sarbu, A.-L. Radu, K. Jankova, A. Daugaard, S. Hvilsted, F.-X. Perrin, M. Teodorescu, C. Munteanu and V. Fruth-Oprisan, *Appl. Clay Sci.*, 2015, **103**, 46–54.

51 R. S. Hebbar, A. M. Isloor, B. Prabhu, Inamuddin, A. M. Asiri and A. F. Ismail, *Sci. Rep.*, 2018, **8**, 4665.
52 S. A. Khan, M. F. Siddiqui and T. A. Khan, *Ultrason. Sonochem.*, 2020, **60**, 104761.
53 F. G. Alabarse, R. V. Conceição, N. M. Balzaretti, F. Schenato and A. M. Xavier, *Appl. Clay Sci.*, 2011, **51**, 202–208.
54 S. Wali, M. I. Khattak, M. I. Khattak and A. Sjjad, *J. Popul. Ther. Clin. Pharmacol.*, 2024, **31**(1), 2022–2033.
55 M. Singha and L. Singh, *Indian J. Pure Appl. Phys.*, 2016, **54**, 116–122.
56 J. Lin, J. Wu, Z. Yang and M. Pu, *Macromol. Rapid Commun.*, 2001, **22**, 422–424.
57 W.-F. Lee and Y.-C. Chen, Effect of intercalated reactive mica on water absorbency for poly(sodium acrylate) composite superabsorbents, *Eur. Polym. J.*, 2005, **41**(7), 1605–1612.
58 M. Selvam, K. Sakthipandi, R. Suriyaprabha, K. Saminathan and V. Rajendran, Synthesis and characterization of electrochemically-reduced graphene, *Bull. Mater. Sci.*, 2013, **36**(7), 1315–1321.
59 M. Ding, H. Su, Y. Li, K. Yang, L. Dang, F. Li and B. Xue, *Mater. Today Chem.*, 2022, **26**, 101049.
60 L. Wu, L. Zeng, L. Chen and H. C. Zhang, *Polym. Bull.*, 2012, **68**, 309–316.
61 W. C. Lin, W. Fan, A. Marcellan, D. Hourdet and C. Creton, *Macromolecules*, 2010, **43**, 2554–2563.
62 H. A. Khonakdar, J. Morshedian and H. Yazdani, *e-Polymers*, 2008, **8**(1), 099.
63 T. Wan, L. Xiong, R. Huang, S. Mengmeng, Q. Lili, T. Xuemei and H. Junyan, *J. Wuhan Univ. Technol., Mater. Sci. Ed.*, 2014, **29**, 1302–1306.
64 W.-M. Cheng, X.-M. Hu, Y.-Y. Zhao, M.-Y. Wu, Z.-X. Hu and X.-T. Yu, *e-Polymers*, 2017, **17**(1), 95–106.
65 V. Penkavova, A. Spalova and J. Tihon, *Mater. Today Commun.*, 2023, **34**, 105150.
66 J. H. Wu, Y. L. Wei and S. B. Lin, *Polymer*, 2003, **44**, 6513.
67 J. Ren, N. Zhan, J. Yang and X. Xiang, *Macromol. Chem. Phys.*, 2023, **224**(22), 2300266.
68 D. M. Devine and C. L. Higginbotham, *Polymer*, 2003, **44**(26), 7851–7860.
69 A. Pourjavadi, Z. Bassampour, H. Ghasemzadeh, M. Nazari, L. Zolghadr and S. H. Hosseini, *J. Polym. Res.*, 2016, **23**(3), 1–10.
70 P. Li, N. H. Kim, Siddaramaiah and J. H. Lee, *Composites, Part B*, 2009, **40**(4), 275–283.
71 F.-M. Preda, A. Alegría, A. Bocahut, L.-A. Fillot, D. R. Long and P. Sotta, *Macromolecules*, 2015, **48**(16), 5730–5741.
72 Y. Zhang, F. Wu, M. Li and E. Wang, *Polymer*, 2005, **46**(18), 7695–7700.
73 Y. M. Mohan, J. P. Dickson and K. E. Geckeler, *Polym. Int.*, 2006, **56**(2), 175–185.
74 S. Azizian, *J. Colloid Interface Sci.*, 2004, **276**, 47–52.
75 Y.-S. Ho and G. McKay, *Process Biochem.*, 1999, **34**, 451–465.
76 C. Aharoni and M. Ungarish, *J. Chem. Soc., Faraday Trans.*, 1976, **1**(72), 400–408.
77 W. J. Weber and J. C. Morris, *J. Sanit. Eng. Div., Am. Soc. Civ. Eng.*, 1963, **89**, 31–60.
78 N. A. Oladoja, *Desalin. Water Treat.*, 2015, **57**(34), 15813–15825.
79 K. V. Kumar, *J. Hazard. Mater.*, 2006, **137**(3), 1538–1544.
80 K. Gayathri and N. Palanisamy, *Sep. Sci. Technol.*, 2019, **55**(2), 266–277.
81 M. J. Ahmed and S. K. Dhedan, *Fluid Phase Equilib.*, 2012, **317**, 9–14.
82 F. Mohammadzadeh, M. Golshan, V. Haddadi-Asl and M. Salami-Kalajahi, *Sci. Rep.*, 2023, **13**(1), 11900.

